Physical Modulation of Intracellular Signaling Processes by Locational Regulation

Jason M. Haugh* and Douglas A. Lauffenburger*#
*Department of Chemical Engineering and #Center for Biomedical Engineering, Massachusetts Institute of Technology, Cambridge, Massachusetts 02139 USA

ABSTRACT Recent observations in the field of signal transduction suggest that where a protein is located within a cell can be as important as its activity measured in solution for activation of its downstream pathway. The physical organization of the cell can provide an additional layer of control upon the chemical reaction networks that govern ultimately perceived signals. Using the cytosol and plasma membrane as relevant compartmental distinctions, we analyze the effect of relocation on the rate of association with a membrane-associated target. We quantify this effect as an enhancement factor E in terms of measurable parameters such as the number of available targets, molecular diffusivities, and intrinsic reaction rate constants. We then employ two simple yet relevant example models to illustrate how relocation can affect the dynamics of signal transduction pathways. The temporal profiles and phase behavior of these models are investigated. We also relate experimentally observable aspects of signal transduction such as peak activation and the relative time scales of stimulus and response to quantitative aspects of the relocation mechanisms in our models. In our example schemes, nearly complete relocation of the cytosolic species in the signaling pair is required to generate meaningful activation of the model pathways when the association rate enhancement factor E is as low as 10; when E is 100 or greater, only a small fraction of the protein must be relocated.

INTRODUCTION

The behavior of living cells is regulated by chemical and/or physical cues from the extracellular environment. Cells may respond by proliferating, differentiating, or migrating in response to diverse chemical stimuli, and may respond differently to varying magnitudes or durations of the same stimulus. Most often, molecular ligands act via an appropriate repertoire of complementary cell surface receptors. What happens next is the initiation of a complicated network of physical and chemical interactions among signaling molecules contained within the cell, a dynamic, integrated system that ensures response fidelity.

A major class of cell surface receptors is the receptor tyrosine kinases (RTKs), which recognize a broad group of growth factor ligands (van der Geer et al., 1994). Because these receptors are integral membrane proteins, subsequent signaling always involves an interaction where at least one of the coupling sites is associated with a two-dimensional surface. After the ligand-dependent auto- and/or transphosphorylation of specific tyrosines in the cytosolic tails of RTKs, signaling molecules can be recruited from the cytosol if they possess appropriate structural domains that directly associate with certain phosphotyrosyl motifs. These include the Src-homology 2 (SH2) and phosphotyrosine-binding (PTB) modular domains (Pawson, 1995). The concept that location matters in cell biology has become prominent (Carraway and Carraway, 1995; Mochly-Rosen, 1995), particularly the notion that location or relocation of a signaling protein can directly affect its observed activity.

As a specific example, homologs of Son of Sevenless (Sos), guanine nucleotide exchange factors (GEFs) specific for the highly conserved Ras GTPase (Bourne et al., 1991), are recruited to the plasma membrane via association with SH2 domain-containing adaptor proteins. GEFs stimulate dissociation of guanine nucleotides (GDP and GTP) from GTPases (Feig, 1994), favoring the active state of a GTPase, because GTP is in excess in the cytosol. Although it was discovered that the coprecipitation of Sos with the phosphorylated RTK epidermal growth factor (EGF) receptor is required for Ras activation mediated by EGF, its GEF activity measured in solution is not affected by the interaction (Buday and Downward, 1993). But when Sos is genetically targeted to the inside face of the plasma membrane, where Ras resides constitutively, cells become transformed in a Ras-dependent fashion in the absence of growth factors (Aronheim et al., 1994; Quilliam et al., 1994). This implies that membrane association causes an increase in the GEF activity of Sos, presumably by allowing better access to its substrate.

In its GTP-bound state, Ras initiates a kinase cascade implicated in cell growth and differentiation by participating in the activation of the cytosolic Raf serine-threonine kinase (Howe et al., 1992; Hallberg et al., 1994). Oncogenic mutations in either Ras or Raf contribute to uncontrolled cellular growth, and Ras mutations in particular have been implicated in a high percentage of human tumors (Bos, 1989). In an unusual twist, when Raf is artificially targeted to the membrane as mentioned above for Sos, cells become

Received for publication 30 August 1996 and in final form 27 January 1997.

Address reprint requests to Dr. D. A. Lauffenburger, Center for Biomedical Engineering, Massachusetts Institute of Technology, Bldg. 66, Room 446, Cambridge, MA 02139. Tel.: 617-252-1629; Fax: 617-252-1651; E-mail: lauffen@mit.edu.

0006-3495/97/05/2014/18 $2.00

transformed, even when a dominant-negative Ras mutant is coexpressed (Leevers et al., 1994; Stokoe et al., 1994). Raf kinase activity is normally enriched in plasma membrane fractions of Ras-transformed cells (Jelinek et al., 1996), yet interactions with Ras or membrane lipids in solution are not sufficient to activate the kinase (Kikuchi and Williams, 1994; Force et al., 1994). Thus relocation of pathway components could serve as a key mechanism governing signal transduction upstream and downstream of Ras.

More recent evidence indicates that plasma membrane targeting of phosphatidylinositol-3′-kinase (PI(3)K), a key enzyme that phosphorylates phosphoinositide lipids, may also be a critical switch in regulating intracellular signaling. PI(3)K exists as a dimer of a catalytic p110 subunit and a regulatory p85 subunit with two SH2 domains that mediate association with activated RTKs (van der Geer et al., 1994). This interaction allows full activity of the p110 subunit on PI(3)K lipid substrates. When constitutively active p110 is artificially targeted to the membrane in the absence of growth factor stimulation, maximum activity is proffered (Klippel et al., 1996), implying that allosteric and locational effects are synergistic in the potentiation of PI(3)K activity. An interaction between p110 and Ras has also been reported, enhancing PI(3)K activity in intact cells, but apparently not in solution (Rodriguez-Viciana et al., 1994).

In this paper we investigate how location can affect the kinetics of interactions between proteins within the framework of signal transduction mediated by a membrane RTK. We have divided the treatment into two major sections. First, we briefly summarize the roles of macro- and microscopic processes of molecular association and how they are influenced by the location of the interacting species. These concepts have been developed elsewhere, primarily for extracellular ligand/receptor interactions (Adam and Delbrück, 1968; Berg and Purcell, 1977; Shoup and Szabo, 1982), and we apply them here in the context of location issues relevant to intracellular signal transduction. We then analyze how relocation of a protein from the cytosol to the membrane can dramatically alter the observed kinetics of signaling processes in idealized but illustrative models of signaling pathways.

BACKGROUND

If proteins are permitted to diffuse freely through space, intermolecular encounters occur randomly. While close enough to form favorable electrostatic and van der Waals interactions, associating macromolecules must align their reactive patches in the correct orientation before diffusing away (Northrup and Erickson, 1992). If k_+ is the second-order rate constant describing diffusive collisions, the observed association rate constant $k_f = \gamma k_+$, where γ is the average probability of capture (Shoup and Szabo, 1982). If the alignment and diffusive separation processes are described by second-order rate constants k_{on} and k_-, respectively, then $\gamma = k_{on}/(k_{on} + k_-)$.

When the alignment of two species is very efficient, almost all encounters result in binding ($\gamma \sim 1$ and $k_f \sim k_+$), and the association is said to be diffusion-limited. When molecules diffuse away rapidly after a collision, many collisions will occur before binding ($\gamma \ll 1$), and there are no detectable spatial concentration gradients of the reactants; in this limit, $k_f \approx k_{on}k_+/k_-$. In an isotropic environment, k_- and k_+ must be equivalent to satisfy the diffusion equation, so k_{on} represents the intrinsic chemical rate constant of the association. Alternatively, close-proximity alignment and separation can be modeled as first-order, unimolecular processes, imposing the existence of a nonspecific encounter complex. This restricts a target from interacting with more than one solute in close proximity, which is nonphysical.

Once associated, the bimolecular complex is not completely stable and can dissociate. If we consider that the complex has an average lifetime, molecular dissociation on a microscopic level is described by a first-order rate constant k_{off}. The probability of rebinding after dissociation is γ, and the observed dissociation rate constant k_r is thus $(1 - \gamma)k_{off}$ (Shoup and Szabo, 1982). Thus, when diffusion matters, the observed rate constants k_f and k_r are modified from their intrinsic values, and the intracellular locations of interacting species can affect the rate of binding.

The observed affinity K, however, is not altered by a change in diffusion rates: $K = k_f/k_r = (\gamma k_+)/[(1 - \gamma)k_{off}] = [(1 - \gamma)k_{on}]/[(1 - \gamma)k_{off}] = k_{on}/k_{off}$ (Lauffenburger and Linderman, 1993). To illustrate this idea, consider a diffusion-limited interaction that has reached equilibrium. At steady state, there is no net formation of bimolecular complexes, so any concentration gradients disappear; the diffusion- and reaction-limited equilibria are therefore indistinguishable. Thus, by analyzing how k_f is affected relative to k_{on}, an analysis of dissociation resistances is not required to ascertain k_r relative to k_{off}. We discuss here these issues as they apply to interactions of cytosolic or membrane-associated proteins with a target displayed on the inside face of the plasma membrane.

Association of a cytosolic protein with a membrane target

To associate with specific targets available on the inside face of the plasma membrane, a cytosolic species must approach the membrane, find a specific site, and bind to this site before diffusing away. The diffusive aspect of this behavior is different from the capture of an extracellular protein by specific cell surface sites (Berg and Purcell, 1977; Erickson et al., 1987; Goldstein, 1989), primarily because cytosolic species are contained by the reactive boundary. We can employ a form of Poisson's equation to solve for the mean time to diffusion-limited capture in space:

$$D_c\nabla^2 W + 1 = 0 \qquad (1)$$

(Berg and Purcell, 1977; Szabo et al., 1980), where W is the mean time to capture and D_c is the molecular diffusivity of the solute in cytosol.

The mean time for first-order diffusion to the boundary can be solved easily for spherical coordinates:

$$\bar{\tau}_1 \equiv \frac{\bar{W}D_c}{a^2} = \frac{1}{15}, \tag{2}$$

where $\bar{W}$ is the capture time averaged over space and a is the cell radius. Because a cytosolic protein cannot diffuse to infinity, this result is lower than that of an extracellular protein diffusing to the outside surface ($\bar{\tau} = 1/3$). When membrane sites are very sparse, diffusion-limited association relies more on finding a site once it is near the surface. The concentration gradients about each of the N uniformly distributed sinks become independent, and the cell radius can be considered semiinfinite. This contribution to the mean capture time is inversely proportional to the number of sinks and depends on the sink geometry:

$$\bar{\tau}_2 = \frac{\pi}{3\sigma N}\,(\text{flat})$$

$$\bar{\tau}_2 = \frac{2}{3\sigma N}\,(\text{hemispherical}) \tag{3}$$

$$\sigma \equiv \frac{s}{a} \ll 1$$

(Hill, 1975; Berg and Purcell, 1977), where the dimension s is the sum of the associating species' radii, the distance r at which the species are in contact. For reasonably sparse sinks, this result compares fairly well with an approximate space-averaged solution of Eq. 1; Poisson's equation was solved with appropriate boundary conditions applied directly to the volume apportioned each sink (Appendix A), approximated as the section of a sphere cut out by the cone $\theta = \beta \equiv b/a$, where b is the mean half-distance between sinks (Fig. 1). To a first approximation, $N = 4/\beta^2$.

The final resistance is the binding of the molecule, now in close proximity to the membrane site:

$$\bar{\tau}_3 = \frac{4\pi a D_c}{3k_{on}N}. \tag{4}$$

In the absence of diffusive resistances in aqueous solution, k_{on} can be measured in the laboratory. However, this may not generalize to what is observed, because the membrane site will be restricted in its ability to orient randomly and/or sample space; thus the entropic contribution of membrane confinement to k_{on} may aid or hinder binding. Constructing a second-order association rate constant $k_{c/m}$ for binding of cytosolic and membrane components (flat sink geometry; based on whole cell volume),

$$k_{c/m} = \left[\frac{N}{20\pi a D_c} + \frac{1}{4sD_c} + \frac{1}{k_{on}}\right]^{-1}. \tag{5}$$

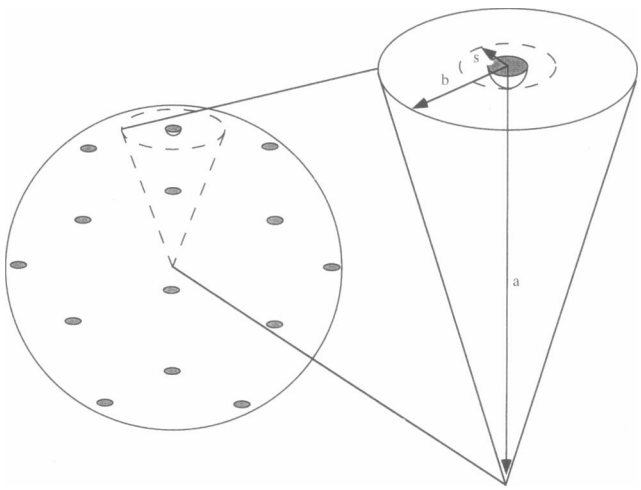

FIGURE 1 Geometry of the area and volume afforded each membrane sink. If we consider a spherical cell of radius a with N targets evenly distributed over the inside surface of the plasma membrane, the area occupied by a single target can by approximated as a disk of radius $b = 2aN^{-1/2}$, the average distance between targets. The targets bind reactant partners at a separation s with observed second-order rate constant k_{on}; s is roughly the sum of the species' molecular radii. The corresponding volume is the section cut out by the cone $\theta = b/a$, with the sink centered at $\theta = 0$.

We can now make order-of-magnitude estimates to gauge the relative importances of molecular processes and set a reasonable upper limit on $k_{c/m}$. The molecular diffusivity of a protein in the cytosol is about two orders of magnitude lower than in aqueous solution, $\sim 10^{-8}$ cm^2/s (Jacobson and Wojcieszyn, 1984; Gershon et al., 1985). For typical cell parameters ($a \approx 10^{-3}$ cm, $s \approx 5 \times 10^{-7}$ cm), $4sD_cN_{Av} \approx 10^7$ (Ms)$^{-1}$ (N_{Av} is Avogadro's number, M denotes concentration in molarity), and the first resistance dominates the second only if $N \gg 30{,}000$. As a relevant example, we can use this reasoning to analyze the recruitment of intracellular signaling proteins to RTKs phosphorylated on tyrosine. As discussed earlier, proteins generally use discrete domains to interact with membrane receptors, exhibiting very high on and off rates and dissociation constants in the 10–100 nM range (Cussac et al., 1994; Ladbury et al., 1995; Zhou et al., 1995; Mandiyan et al., 1996). Given the above analysis, recruitment is likely diffusion limited, with a forward rate constant of $\sim 10^7$ (Ms)$^{-1}$ based on the whole cell volume and a reverse rate constant in the 0.1–1 s^{-1} range. To compare these rates to those governing RTK ligand binding, the aforementioned EGF-receptor/EGF system exhibits forward and reverse binding constants of $\sim 10^6$ (Ms)$^{-1}$ and ~ 0.005 s^{-1}, respectively (Lauffenburger and Linderman, 1993). Recruitment of cytosolic proteins would thus respond rapidly to receptor binding, establishing new equilibria as receptor occupancy changes with time (pseudoequilibrium).

Interaction between two membrane species

If the number of sinks, N, stays relatively constant on the time scale of membrane diffusion, we can characterize

association with a second membrane species as we did in the previous section. We approximate the area afforded each sink as a flat circular disk of radius b, and the species react at a distance $r = s$.

One approach is to employ Eq. 1 to find the mean capture time of the second membrane species. Solving for W and averaging over space,

$$\bar{\tau} \equiv \frac{\bar{W}D_m}{b^2} = \frac{1}{2}\left[\frac{\ln(1/\tilde{s})}{(1-\tilde{s}^2)} - \frac{(3-\tilde{s}^2)}{4}\right]; \quad \tilde{s} \equiv s/b = \sigma/\beta \tag{6a}$$

(Berg and Purcell, 1977), where D_m is the sum of the species' membrane diffusivities. With D_m in the 10^{-11}–10^{-9} cm^2/s range, proteins are less mobile in the plasma membrane than in the cytosol; however, the change in distance scales from a to b ($b \ll a$ in general) and a reduction in dimensionality mean that the transport rate is not necessarily reduced by membrane association.

A more complicated expression can be used that accounts for spherical curvature:

$$\bar{\tau} = \frac{1}{2\beta^2}\left\{\frac{(1-\eta_b)^2}{(\eta_s-\eta_b)}\ln\left(\frac{1-\eta_b}{1-\eta_s}\right) - \left[2 - \frac{(1+\eta_b)^2}{(\eta_s-\eta_b)}\ln\left(\frac{1+\eta_s}{1+\eta_b}\right)\right]\right\}; \quad \begin{matrix}\eta_b \equiv \cos\beta \\ \eta_s \equiv \cos\sigma\end{matrix} \tag{6b}$$

However, even for $\beta \sim 1$, Eq. 6a differs from this result by $<10\%$.

A more accurate determination of $\bar{\tau}$ is made by first solving the diffusion equation with appropriate boundary conditions for the dimensionless concentration profile $\theta(r,t)$, again assuming that changes in b are imperceptible on the b^2/D_m time scale (<1 s in general):

$$\bar{\tau} \equiv \frac{\bar{W}D_m}{b^2} = \frac{2}{(1-\tilde{s}^2)}\sum_{n=1}^{\infty}\frac{2}{\lambda_n^4}\left[\frac{J_1^2(\lambda_n)}{J_0^2(\lambda_n\tilde{s}) - J_1^2(\lambda_n)}\right]; \quad J_0(\lambda_n\tilde{s})Y_1(\lambda_n) - J_1(\lambda_n)Y_0(\lambda_n\tilde{s}) = 0, \tag{7}$$

where J_n and Y_n are Bessel functions (Adam and Delbrück, 1968). Computational analysis of Eq. 7 shows excellent agreement with Eq. 6a for a wide range of target densities, and the extent that $\bar{\theta}(t) \approx \exp(-t/\bar{W})$ depends on the dominance of the first term in Eq. 7 ($1/\tau \approx \lambda_1^2$). Furthermore, modifying the boundary condition at the sink to include a second-order reactive rate constant k_2 confirms the intuition that the observed second-order rate constant between membrane species can be constructed by analogy to serial resistances in an electrical circuit:

$$\tilde{s}\left.\frac{\partial\theta}{\partial\tilde{r}}\right|_{\tilde{s}} - \kappa\theta|_{\tilde{s}} = 0; \quad \kappa \equiv \frac{k_2}{2\pi D_m}$$

$$\bar{\tau} = \frac{2}{(1-\tilde{s}^2)}\sum_{n=1}^{\infty}\frac{2}{\lambda_n^4}\cdot\left\{\frac{\kappa^2 J_1^2(\lambda_n)}{[(\lambda_n\tilde{s})J_1(\lambda_n\tilde{s}) + \kappa J_0(\lambda_n\tilde{s})]^2 - [(\lambda_n\tilde{s})^2 + \kappa^2]J_1^2(\lambda_n)}\right\}$$

$$\lambda_n\tilde{s}[J_1(\lambda_n)Y_1(\lambda_n\tilde{s}) - J_1(\lambda_n\tilde{s})Y_1(\lambda_n)] - \kappa[J_0(\lambda_n\tilde{s})Y_1(\lambda_n) - J_1(\lambda_n)Y_0(\lambda_n\tilde{s})] = 0$$

$$\bar{\tau} = \bar{\tau}(\kappa \to \infty) + \frac{(1-\tilde{s}^2)}{2\kappa}. \tag{8}$$

Note that k_2 is analogous to k_{on}, except for the change in units to reflect concentrations in two dimensions rather than three. Again, we cannot say in general how membrane association will affect the efficiency of alignment when the associating species are in close proximity. However, when associations are reaction-limited, we stipulate that the primary effect of membrane confinement is a change in the effective sampling volume ($V_{sampling}$) to a value much smaller than the whole cell (V_{cell}). Using order-of-magnitude reasoning, we can approximate $V_{sampling}$ as a layer adjacent to the membrane of thickness $h \approx 10$ nm (Lauffenburger and Linderman, 1993; McLaughlin and Aderem, 1995), and we define the reaction-limited enhancement factor as χ:

$$\chi \approx \frac{V_{cell}}{V_{sampling}} \approx \frac{a}{3h} \approx 10^2 \text{ to } 10^3. \tag{9}$$

Furthermore, the dissociation rate k_{off} is unaffected by a change in volume, so the apparent affinity is enhanced by the factor χ, even when diffusive resistances are important.

Constructing an observed second-order rate constant based on the whole cell volume for association of membrane species

$$k_{m/m} \approx \left\{\frac{3}{2\pi a D_m}[\ln(1/\tilde{s}) - 3/4] + \frac{1}{\chi k_{on}}\right\}^{-1}; \quad \tilde{s}^2 \ll 1. \tag{10}$$

The diffusion-limited value of $k_{m/m}$ is $\sim 10^6$–10^8 (Ms)$^{-1}$, depending mainly on D_m and weakly on $\tilde{s} = 2\sigma N^{-1/2}$. This estimate clearly qualifies the statement that the reduction in mobility does not preclude a reduction in the frequency of collisions. For typical χk_{on} values in the range of 10^7–10^{10} (Ms)$^{-1}$, we see that $k_{m/m}$ is diffusion-limited for all but the slowest reactions and/or most mobile reactants (Lauffenburger and Linderman, 1993).

MODELS, ANALYSES, AND RESULTS

Two major implications of membrane compartmentalization, compared with cytosolic interactions, are 1) that the apparent binding affinity is enhanced by the factor χ (Eq. 9), by at least two orders of magnitude, and 2) that the association rate, gauging the response time to an extracellular stimulus perceived by a membrane receptor, can be increased considerably. In any given situation, however, it is not obvious whether enhancement of the association rate is due to a reactant-concentrating effect (Nesheim et al., 1984)

or to the high efficiency of diffusion in two dimensions (reduction-of-dimensionality), even when the molecular diffusivity is reduced. To address the how and why of "location matters," it is instructive to compare the second-order rate constants for cytosolic and membrane species interacting with a membrane target.

We introduce here an enhancement factor E, which compares $k_{m/m}$ and $k_{c/m}$ as described in the previous section:

$$E \equiv \frac{k_{m/m}}{k_{c/m}}. \tag{11}$$

E thus quantifies the advantage of relocation from the cytosol to the plasma membrane conferred in the binding of a constitutively membrane-associated target. We further define two other dimensionless variables: a cellular Damköhler number Da comparing the contributions of reaction and diffusion to $k_{c/m}$:

$$\mathrm{Da} \equiv \frac{k_{on}}{k_{c/m}(k_{on} \to \infty)} = \frac{k_{on}}{aD_c}\left(\frac{N}{20\pi} + \frac{1}{4\sigma}\right), \tag{12}$$

and a physical parameter δ, which compares the diffusion-limited values of $k_{m/m}$ and $k_{c/m}$:

$$\delta \equiv \frac{k_{m/m}(k_{on} \to \infty)}{k_{c/m}(k_{on} \to \infty)} \approx \frac{D_m}{D_c}\left[\frac{N/5 + \pi/\sigma}{6\ln(1/\tilde{s}) - 9/2}\right]. \tag{13}$$

By our previous order-of-magnitude reasoning, Da = 1 corresponds to $k_{on} \sim 10^7\ (\mathrm{Ms})^{-1}$, or less if $N > 10^5$. Because $\tilde{s} = 2\sigma N^{-1/2}$, δ is a function of the relative mobility in the membrane versus cytosol (D_m/D_c), target availability (N), and molecular versus cellular dimensions (σ). The dependence of δ on N is illustrated for $D_m/D_c = 0.001$–0.1 and $\sigma = 5 \times 10^{-4}$ in Fig. 2 *A*. Note that δ is often much greater than 1, even when D_m/D_c is well below 1. This again underscores the efficiency of diffusion in two dimensions.

We can now express E in terms of Da, δ, and the previously defined χ:

$$E = \chi\left[\frac{1 + \mathrm{Da}}{1 + (\chi/\delta)\mathrm{Da}}\right]. \tag{14}$$

The curve described by Eq. 14 is sigmoidal in shape with asymptotic values of χ and δ as k_{on} approaches zero (reactant concentrating effect) and infinity (diffusion effects only), respectively (Fig. 2 *B*). From Fig. 2 *A*, δ is bounded between ~0.1 and 10^3. Thus, for reaction-limited associations, $E = \chi$, and E can be $\sim\chi$ or <1 for species that bind rapidly upon encounter, depending on D_m and N.

The interaction of a cytosolic protein with a membrane target can be considered reaction-limited for Da < 0.1 and diffusion-limited for Da > 10. For interactions between two membrane species, $(\chi/\delta)\mathrm{Da} \approx 0$ describes reaction-limited behavior, whereas $(\chi/\delta)\mathrm{Da} > 10$ describes diffusion-limited associations. Thus the representation of E in Eq. 14 allows the enhancement effect to be visualized easily with a minimum of free variables, and it allows us to segment Fig. 2 *B* into regimes in which chemical and physical cell parameters

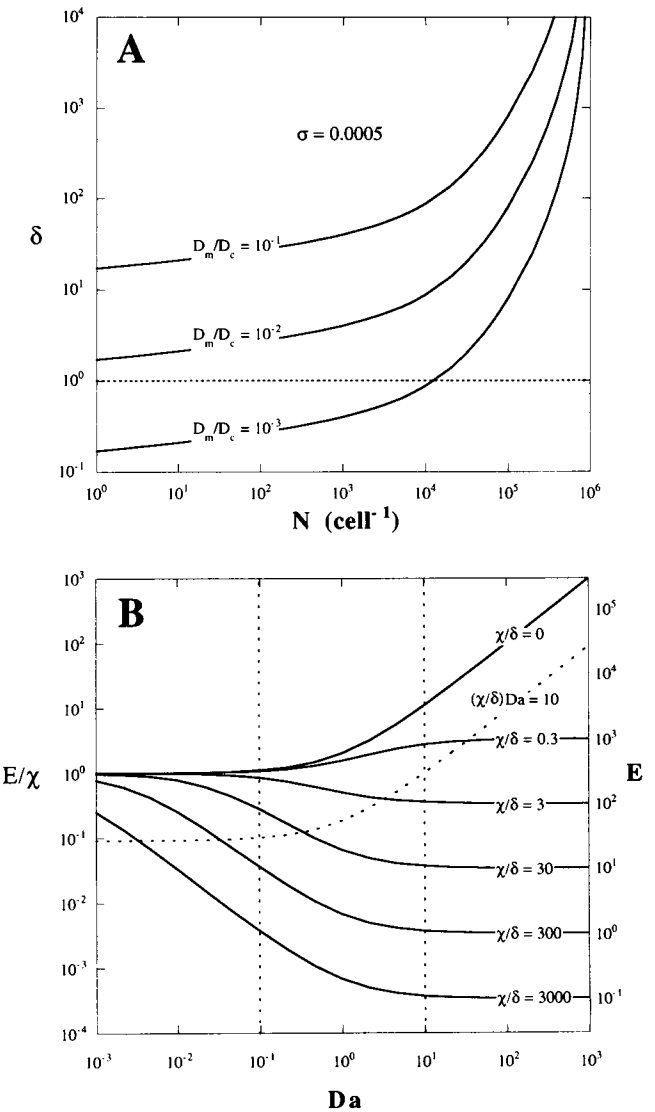

FIGURE 2 Predicted enhancement of kinetic association rate by relocation to the plasma membrane. (*A*) The physical parameter δ, as described in the text, compares the diffusion-limited rates of binding for the association of a specific membrane target with membrane-associated and cytosolic proteins. δ is a function of relative mobility (D_m/D_c), target availability (N), and molecular dimensions (σ), and is plotted versus N for $\sigma = 5 \times 10^{-4}$ and D_m/D_c values of 0.1, 0.01, and 0.001. The entire range of N is explored, and so $\tilde{s}^2$ is not neglected relative to ~1 as in Eq. 13. (*B*) The enhancement factor E compares the rates at which a membrane target is bound by membrane and cytosolic reactant partners (Eq. 14). E is plotted versus a Damköhler number Da, the ratio of mean reaction and diffusion rates when the reactant partner is cytosolic. As Da approaches zero, E simply reflects a reduction in sampling volume, concentrating the reactant by a factor χ. By order-of-magnitude analysis, $E \approx 10^2$–10^3 in this limit (taken to be 300 here). As Da approaches infinity, E approaches δ, the ratio of diffusion-limited binding rates for cytosolic and membrane-binding partners. Whereas Da gauges the importance of diffusion in cytosol-membrane interactions, $(\chi/\delta)\mathrm{Da}$ serves the same purpose for membrane-membrane coupling. For reaction-limited membrane-membrane interactions, $(\chi/\delta)\mathrm{Da} \ll 1$; for diffusion-limited membrane-membrane interactions, $(\chi/\delta)\mathrm{Da} \gg 1$.

contribute differently to $k_{m/m}$ and $k_{c/m}$. Once the effect on the observed forward rate constant is determined, the effect on a reverse rate constant can be determined easily; the enhancement factor will be E/χ, yielding the aforementioned factor of χ enhancement of the observed affinity potentiated by membrane confinement. Fig. 2 *B* shows that E/χ is actually <1 for most cases, meaning that the off rate is generally lower when both reactants are membrane-associated.

If one of two interacting species is permanently associated with the plasma membrane, we can see how the location of the second molecule can matter in signal transduction. For more direct clarification, we present two simple signaling models to illustrate the potential impact of locational control (Fig. 3). Each model involves responses to stimulation of a membrane receptor with a constant extracellular concentration of agonist. As a very well characterized system, the typical binding and internalization kinetics of EGF receptor will be used (Appendix B). EGF receptor occupation at the surface is very dynamic on the time scale of minutes. For simplicity we neglect receptor synthesis, recycling, and nonspecific (constitutive) internalization, as well as feedback attenuation of the receptor kinase. These are valid assumptions for the first 10–15 min of stimulation, a time scale over which many signaling molecules show dramatic activation profiles. We also discount signaling from receptor-ligand complexes in an endosomal compartment, which brings up distinct signal compartmentalization issues (Baass et al., 1995); these are addressed in Appendix C. The point of our receptor activation model is to be simple and dynamic, not to completely capture all of the nuances of receptor trafficking and compartmentalization or to suggest any long time-scale implications.

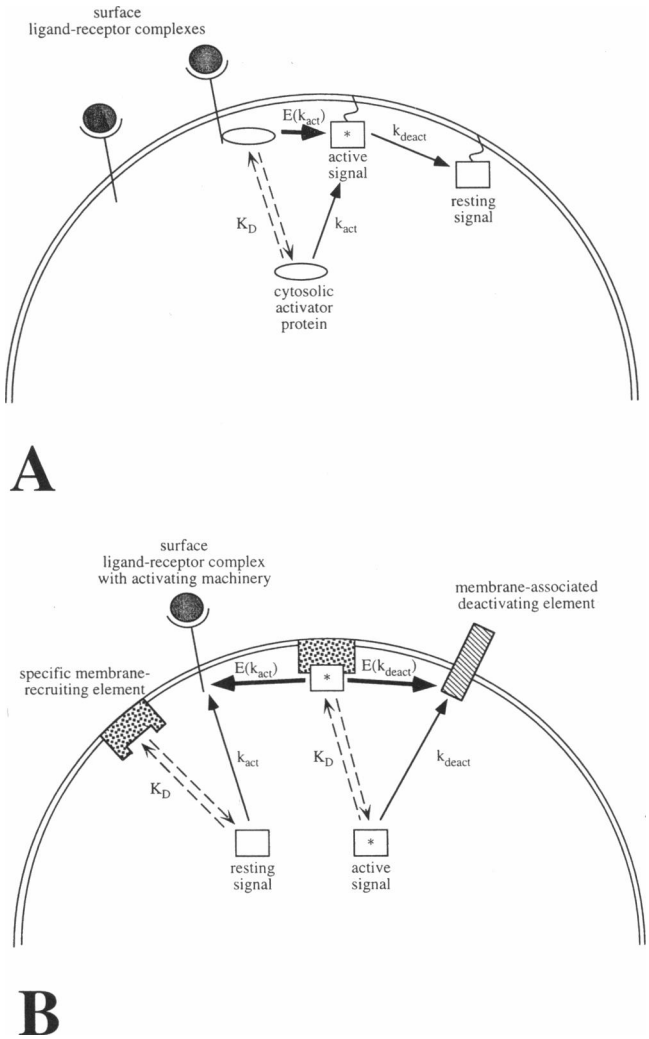

FIGURE 3 Two highly simplified signal transduction models. (*A*) Model 1. The first model involves the signaling through a membrane-associated molecule regulated by distinct cytosolic activating and deactivating proteins. The baseline activation is small but is up-regulated by the accumulation of surface receptor-ligand complexes able to specifically recruit only the activating element to the plasma membrane. This recruitment is in pseudoequilibrium with the level of receptor occupancy, and is characterized by dissociation constant K_D. Because the specific activity of the activating protein varies depending on location, we model activation as a second-order process with constitutive rate constant k_{act}. With the activating element and molecule of interest both at the membrane, the observed rate of activation is enhanced by a factor E, as described in the text. Because the specific activity of the deactivating protein is considered constant, we model deactivation as a first-order process with observed rate constant k_{deact}. (*B*) Model 2. The second model is concerned with a cytosolic signaling protein regulated by distinct, constitutively membrane-associated elements. The activating element is the enzymatic action of bound receptors. We again model activation and deactivation of the signal as second- and pseudo-first-order processes with observed rate constants k_{act} and k_{deact}, respectively. Relocation of the cytosolic signal to the plasma membrane is mediated by specific membrane sites, an interaction in pseudoequilibrium characterized by dissociation constant K_D. By relocating the signaling protein to the membrane, the activation and deactivation rates are enhanced by the same factor, but the regulation of the signal becomes more efficient by responding much faster to changes in the extracellular input.

Model 1: up-regulation of a membrane messenger by a membrane receptor-recruited activator

Model 1 describes the regulation of a constitutively membrane-associated signaling protein by two distinct cytosolic activating and deactivating proteins. The fraction of our signaling protein in the active state is at a low baseline steady-state value for $t < 0$. In this scheme, a cell surface receptor bound to an extracellular agonist can up-regulate the signal by recruiting only the activator to the plasma membrane via interactions with its intracellular tail (Fig. 3 *A*). This model therefore illustrates how specific relocation can mediate a signal by differentially modulating competing mechanisms that alter the activation state of a membrane-associated protein.

The levels of all proteins on our time scale of interest are conserved. The net rate of change in the activation state of the signaling protein is expressed in terms of activating and deactivating fluxes. The switch to the effector state occurs rapidly after the binding of activating and signaling proteins. In terms of Michaelis-Menten enzyme kinetics parameters, this means that product formation is always in the linear range, with observed second-order rate constant

$k_{cat}/K_M = k_f k_{cat}/(k_r + k_{cat}) \approx k_f$. To generalize for other modeling considerations, membrane confinement affects only the Michaelis constant K_M when product leaving rates are unaffected (Gentry et al., 1995); if k_f and k_r are the observed association and dissociation rate constants observed for a cytosol-membrane pair, then $K_M = (Ek_r/\chi + k_{cat})/Ek_f$ (based on whole cell volume) after relocation of the cytosolic protein to the membrane.

Because the specific activity of the activating protein is not constant, we model the activation flux as a second-order process. We consider the specific activity of the deactivating protein to be constant for all time, so the deactivating flux is pseudo-first-order. Defining α to be the fraction of our protein of interest in the activated state, the baseline activation level is

$$\alpha_0 = \frac{k_{act}A_T}{k_{act}A_T + k_{deact}}, \tag{15}$$

where k_{act} and k_{deact} are the rate constants of activation and deactivation observed in the absence of ligand, respectively, and A_T is the total number of activator molecules in the cell. At $t = 0$, a constant concentration of agonist is added, and the activator is recruited with rapid kinetics compared to agonist binding (pseudoequilibrium). Employing mass-action kinetics, the net rate of protein activation is

$$\dot{\alpha} = k_{act}A_T\left\{1 + (E-1)\left[\frac{C_s(t)}{K_D + C_s(t)}\right]\right\}(1-\alpha) - k_{deact}\alpha, \tag{16}$$

where $C_s(t)$ is the level of receptor-agonist complexes displayed at the cell surface (see Appendix B for a description of the kinetics), and K_D is the dissociation constant describing the equilibrium between surface complexes and the recruited activator. The initial condition for Eq. 16 is given by Eq. 15. Because we have assumed that receptor function is not affected by intracellular feedback loops on the time scales we are investigating, $C_s(t)$ is an external, independent function of time separable from downstream signaling. E is the enhancement factor due to membrane translocation, as described by Eq. 14. Although E can be a function of $C_s(t)$, we set it to a constant value for simplicity.

Because $C_s(t)$ does not depend on α, Eq. 16 is linear; nevertheless, we rapidly solved it numerically to within 0.001% using the LSODE subroutine (Hindmarsh, 1980) on a Sun workstation. The activation profiles α versus t and phase diagrams $\alpha(t)$ versus $C_s(t)$ are displayed in Fig. 4 for reasonable parameter values and various values of λ, the dimensionless extracellular ligand concentration. The activation profiles of α (Fig. 4 *A*) are similar to that of C_s, which is to be expected if the pattern of ligand stimulation is to have a controllable effect on the resulting signal. The peak value of α saturates with λ much as C_s does.

More telling information, however, lies in the phase diagram of α versus C_s (Fig. 4 *B*). We can visualize the interplay between receptor and messenger and the disparity between time scales without seeing time pass explicitly. On extremely short time scales (seconds or less), $\Delta\alpha \approx \Delta C_s \approx 0$, and the differential equations can be approximated by difference equations:

$$\frac{\Delta\alpha}{t} \approx k_{act}A_T(E-1)(1-\alpha_0)\left(\frac{c}{\kappa + c}\right); \quad c \equiv \frac{C_s}{R_0}; \quad \kappa \equiv \frac{K_D}{R_0}$$

$$\frac{c}{t} \approx \lambda k \tag{17}$$

$$\Delta\alpha \approx (E-1)\left(\frac{1-\alpha_0}{\lambda}\right)\left(\frac{k_{act}A_T}{k_r}\right)\left[c - \left(\frac{\kappa c}{\kappa + c}\right)\right],$$

where R_0 is the surface receptor level per cell at $t = 0$, and k_r is the rate constant of ligand dissociation from receptors. Note that C_s and K_D have been nondimensionalized in terms of R_0. As λ is increased, the value of C_s reached by the cell before α responds increases exponentially. The ratio $(E-1)k_{act}A_T/\kappa k_r\lambda$ can be thought of as a response coefficient, and when it is very low, signaling cannot keep up with what is perceived by the signaling machinery as a step change in the occupied receptor level.

Although the above analysis is instructive, it does not capture the shape of the phase diagrams for even the shortest time scales of interest, particularly if λ is large. A more robust equation is found by linearizing Eq. 16 in terms of α and C_s and exploiting the fact that $C_s(t)$ can be expressed as a single exponential for short time scales (Appendix B):

$$\alpha - \alpha_0 \approx \left(\frac{E-1}{\kappa}\right)\left(\frac{k_{act}A_T}{k_r}\right)\left(\frac{1-\alpha_0}{\zeta - g(\lambda)}\right) \cdot\left\{c - \frac{\lambda}{\zeta}\left[1 - \left(1 - \frac{g(\lambda)}{\lambda}c\right)^{\zeta/g(\lambda)}\right]\right\} \tag{18}$$

$$\zeta \equiv \frac{k_{act}A_T + k_{deact}}{k_r}; \quad g(\lambda) \equiv \sqrt{(1+\lambda+\epsilon)^2 - 4\lambda\epsilon},$$

where ϵ is the ratio of the endocytic rate constant k_e to k_r, as defined in Appendix B. Agreement of Eq. 18 with the phase diagrams at the beginning of their trajectories is illustrated in Fig. 4 *B*. On much longer time scales, the signal tends toward pseudoequilibrium with C_s:

$$\alpha_{eq} = \frac{k_{act}A_T(\kappa + Ec)}{k_{act}A_T(\kappa + Ec) + k_{deact}(\kappa + c)}; \tag{19}$$

$$\left(\frac{\alpha_{eq}}{1-\alpha_{eq}}\right) = \left(\frac{\alpha_0}{1-\alpha_0}\right)\left(\frac{1 + Ec/\kappa}{1 + c/\kappa}\right).$$

Thus all trajectories in our model system eventually collapse onto one curve in phase space, as seen in Fig. 4 *B*.

Model 2: responsive activation of a cytosolic messenger by a membrane receptor

The second model describes a cytosolic signaling protein that is regulated by distinct membrane-associated activating and deactivating elements. Thus, compared to Model 1, the

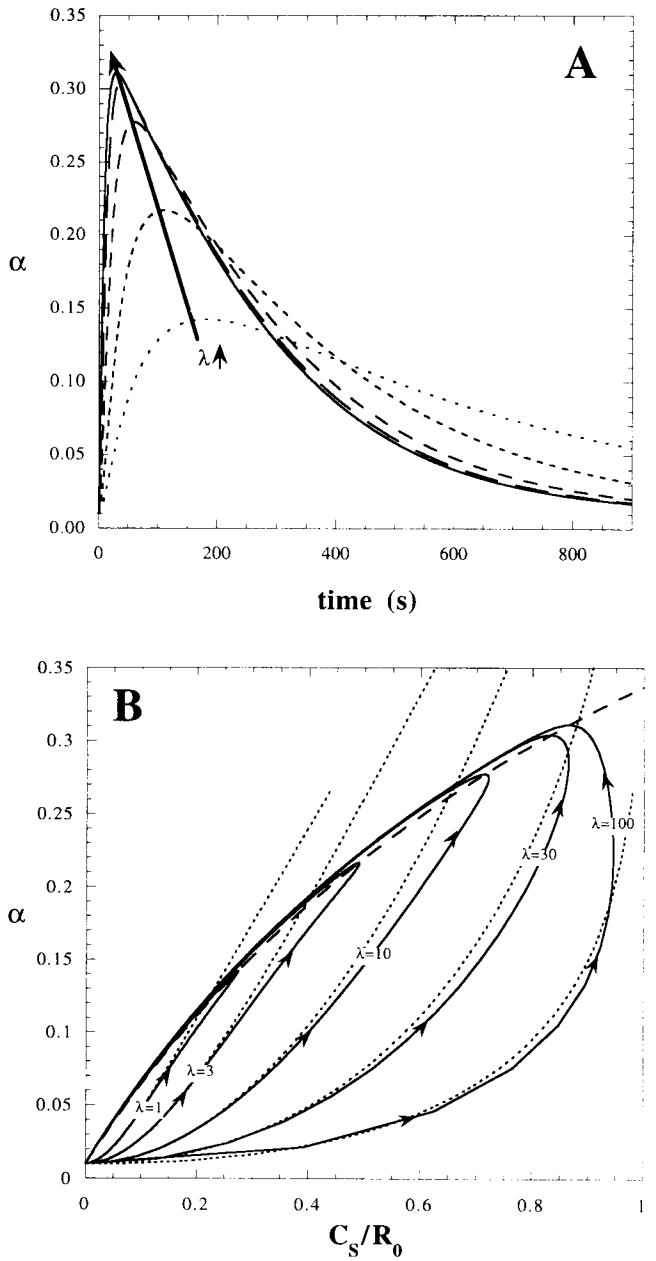

FIGURE 4 Effect of relocation on the up-regulation of a membrane signaling messenger. (*A*) Activation profiles. Equation 16 was solved numerically for the following constant parameter values defined in the text: $k_{act}A_T = 0.001\ s^{-1}$; $k_{deact} = 0.1\ s^{-1}$; $E = 300$; $K_D/R_0 = 5$. The function $C_s(t)$ used is as described in Appendix B, with $k_r = 0.005\ s^{-1}$, $\epsilon = 1$, and λ values of 1, 3, 10, 30, and 100. (*B*) Phase diagrams. The profiles of $\alpha(t)$ and $C_s(t)$ from *A* are combined to make time an implicit variable. If we consider how the curves develop from the beginning to the end of the simulation, each path is a trajectory, with its direction marked by arrows. The dotted lines represent the analytical solution valid for short times (Eq. 17) for the various values of λ. The dashed line denotes the path of pseudoequilibrium (Eq. 18).

locations of the signal and regulatory proteins in the cell's resting state are reversed. The activating element is the enzymatic machinery of occupied surface receptors. This model is meant to illustrate how the relocation of the cytosolic signal to the plasma membrane can streamline its responsiveness to the regulatory elements governing its activation, particularly because the activating element $C_s(t)$ is changing dynamically with time (Fig. 3 *B*).

The cytosolic signal in the unactivated state and surface receptor-ligand complexes interact with second-order rate constant k_{act}, and activation is rapid after association. The specific activity of the membrane-associated deactivating protein is again constant, yielding a pseudo-first-order flux with rate constant k_{deact}. At $t = 0$, the concentration of extracellular agonist is stepped up from zero to a constant value. First let us consider the dynamics of signal generation in the absence of relocation mechanisms. Employing mass-action kinetics,

$$\dot{\alpha} = k_{act}C_s(t)(1 - \alpha) - k_{deact}\alpha \qquad \alpha(0) = 0, \quad (20)$$

where α is again the fraction of our signaling protein in the active state, and $C_s(t)$ is as described in Appendix B.

We will now allow recruitment of the cytosolic protein to the membrane via association with S specific sites, an interaction in pseudoequilibrium with respect to extracellular ligand binding and characterized by dissociation constant K_D. If the activation and deactivation fluxes exhibit the same enhancement factor E due to relocation of the cytosolic substrate of interest, then

$$\dot{\alpha} = \left[1 + (E - 1)\left(\frac{S}{K_D + S}\right)\right]\dot{\alpha}(S = 0), \quad (21)$$

where $\dot{\alpha}(S = 0)$ is given in Eq. 20. While the recruitment of the signaling protein can certainly be regulated by the cell, we consider S to be constant for simplicity, allowing us to lump the variables in brackets into a dimensionless sensitivity parameter η:

$$\eta \equiv \left[1 + (E - 1)\left(\frac{S}{K_D + S}\right)\right]. \quad (22)$$

Thus the relative magnitudes of the activation and deactivation fluxes move in concert. At equilibrium of C_s and α, membrane recruitment does not affect the steady-state value of α, but rather potentiates a rapid response to the transient peak in C_s.

The dynamics of α were again determined numerically; activation profiles and phase diagrams for this case are displayed as Fig. 5 for values of k_{act} and k_{deact} expressly chosen to be relatively unresponsive compared to the binding kinetics of EGF. This time we vary the sensitivity parameter η while keeping $C_s(t)$ constant ($\lambda = 1$). For very short time scales we again convert the differential equations into approximate algebraic expressions to gauge the importance of our variables to the phase behavior at the beginning of the trajectories in Fig. 5 *B*. The gain is, of course,proportional to η:

$$\alpha \approx \frac{\eta k_{act}R_0}{\lambda k_r}\left(\frac{C_s}{R_0}\right)^2. \quad (23)$$

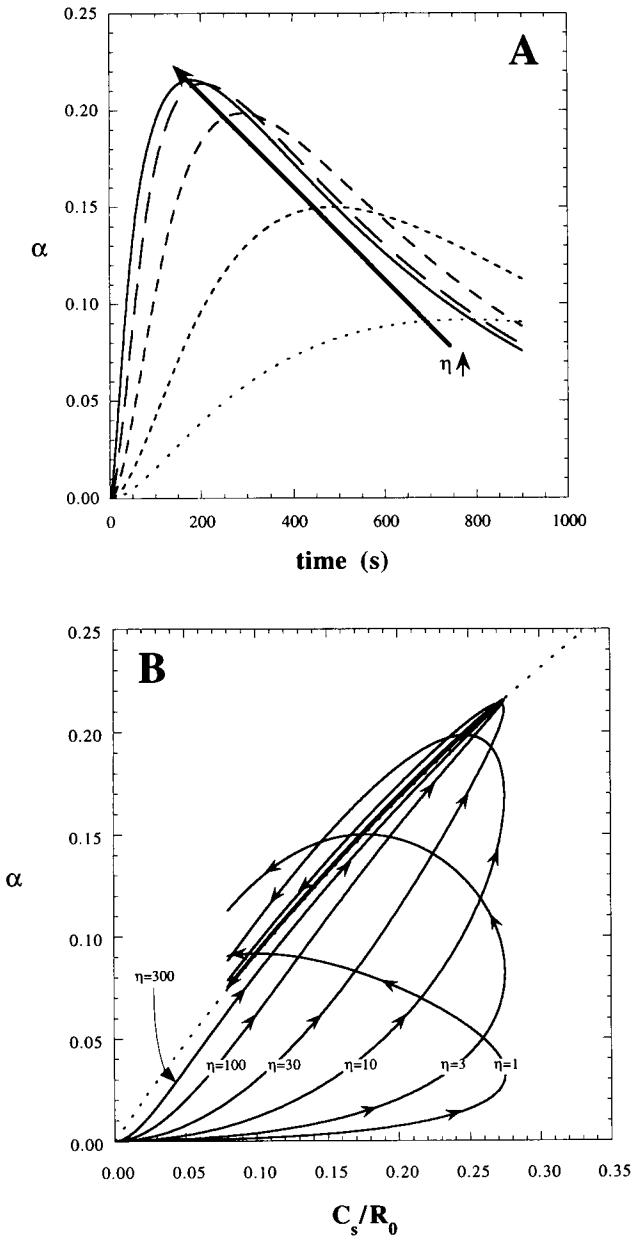

FIGURE 5 Effect of relocation on the responsiveness of signal transduction. (*A*) Activation profiles. Equation 21 was solved numerically for the following constant parameter values defined in the text: $k_{act}R_0 = 0.001$ s^{-1}; $k_{deact} = 0.001$ s^{-1}. The function $C_s(t)$ used is as described in Appendix B, with $k_r = 0.005$ s^{-1}, $\lambda = 1$, and $\epsilon = 1$. The parameter η, which quantifies the sensitivity of $\alpha(t)$ to changes in $C_s(t)$, was varied using the following values: $\eta = 1$, 3, 10, 30, 100, and 300. (*B*) Phase diagrams. The profiles of $\alpha(t)$ and $C_s(t)$ from *A* are combined to make time an implicit variable. If we consider how the curves develop from the beginning to the end of the simulation, each path is a trajectory, with its direction marked by arrows. The dashed line denotes the path of pseudoequilibrium (Eq. 24).

In this case our response coefficient is $\eta k_{act}R_0/\lambda k_r$ (a more robust short-time estimate can be solved using the same technique as with Eq. 18 for Model 1; this is not shown here because we have already demonstrated its applicability). For $\eta \sim 1$, it is clear that in the characteristic time it takes to accumulate α, C_s has already gone through its dynamic. The signal fails to reach a good peak value, although the response observed is more sustained on the time scale of receptor down-regulation (Fig. 5 *A*). For $\eta k_{act}R_0/\lambda k_r \gg 1$, the signaling machinery responds immediately to what it perceives as a slow change in C_s, constantly establishing new pseudoequilibria:

$$\alpha_{eq} = \frac{k_{act}C_s}{k_{act}C_s + k_{deact}}. \tag{24}$$

As η approaches infinity, the signal peaks and down-regulates alongside the level of bound receptors at the surface, and we see the phase trajectories in Fig. 5 *B* get tighter and tighter about Eq. 24. The signal becomes a better translation of the receptors' enzymatic activity, a more efficient transducer of an extracellular instruction. Translocation in this case favors neither the activation nor the deactivation flux, but the behavior can be altered dramatically if the rate constants governing the signal in the absence of relocating mechanisms are on the same order of magnitude or less than those regulating receptor dynamics.

Experimental relevance

We have explained how relocation from the cytosol to the plasma membrane can be used as a cellular switch to affect changes in the magnitude or responsiveness of signal activation, and we have theoretically quantified these effects for typical cellular parameters. However, in an experimental situation in which signal activation is measured, the relevance of this kind of analysis may not be apparent. There is often only a qualitative model of signal regulation, and the generation of multiple time courses for various conditions is often neither practical nor necessary. A singular measure of signal activation is usually sufficient to make quantitative comparisons among different variations of an experiment. Thus we aim to extend our analysis by relating practically accessible observables to various magnitudes of the relocation effect when signal activation is at least qualitatively similar to model 1 or 2. To do this, we generalize for different values of the relocation enhancement factor E; we have shown that E can vary by orders of magnitude, but that a fair estimate of E can be ascertained when D_m and k_{on} can be approximated for a given signaling context.

For signaling similar to model 1, a convenient measure of activation is the maximum value of α attained after stimulation. The peak value α_{max} will experience the best signal-to-noise ratio and is most dramatic compared to the baseline level of signaling α_0. Signaling can be quantified as "fold-activation" relative to a control with no stimulus, measured at a common time after agonist addition, which is characteristic of the peak level reached before down-regulation/desensitization. The dependence of this level of activation on ligand concentration is then considered the dose response of the signal. Although the exact time of the peak will likely differ for different ligand concentrations, this type of data

representation is conceptually easy to understand and experimentally feasible.

For model 1, the fold-activation α_{max}/α_0 obeys Eq. 19 and is therefore a function of $k_{deact}/k_{act}A_T$, E, and the fractional recruitment experienced at the time of peak activation. We define the latter parameter as ϕ; in model 1, we gave $\phi(t)$ a saturable dependence on $C_s(t)$:

$$\phi = \frac{c}{\kappa + c}. \tag{25}$$

Note that because the peaks of C_s and α do not necessarily coincide, the value of ϕ seen at α_{max} is usually not the maximum recruitment $c_{max}/(\kappa + c_{max})$. α_{max}/α_0 for model 1 is plotted versus E for various values of ϕ and $k_{deact}/k_{act}A_T$ = 100, as in Fig. 6. Also noted on the graph are dose-response values attained for E = 300 and the kinetic parameters used in Fig. 4. Although it is intuitive that as E increases, the requirement for recruitment ϕ decreases, Fig. 6 shows the sensitivity of this requirement for an observed α_{max}/α_0. For $E \approx 10$, note that activation of several-fold requires significant recruitment of the activating protein. For $E > 100$, however, only a small percentage of the activating protein must be recruited to get significant activation over baseline (for fivefold enhancement, E = 10 requires ~50% recruitment, E = 100 only ~4%). This can be important, depending on the nature of the recruitment. Often only a small percentage of SH_2 or PTB domain-containing proteins coprecipitate with RTKs or the particulate fraction in general.

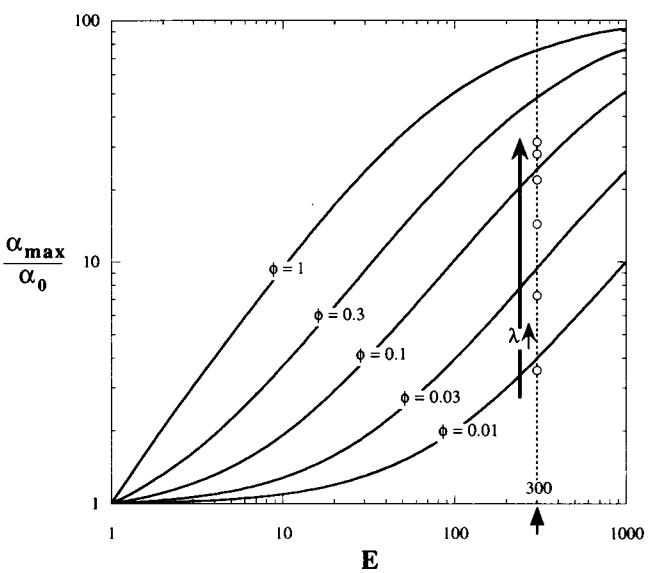

FIGURE 6 Observable sensitivity of Model 1 signal magnitude to changes in relocation mechanism. The maximum level of activation in Model 1 for a constant extracellular agonist concentration is defined as α_{max}, and α_{max}/α_0 represents the "fold-activation" of the signal, a common representation of experimental data in signal transduction. The fraction ϕ of the cytosolic activator recruited to the membrane at the time of peak activation is directly dependent on the dose of ligand in this model, and the enhancement in specific activity at the membrane E depends on the signaling context. α_{max}/α_0 is plotted versus E for various values of ϕ experienced at peak activation ($k_{deact}/k_{act}A_T$ = 100), gauging the sensitivity of the signal to aspects of relocation. Circular symbols mark the dose-response behavior of the model for the following parameters as used in Fig. 4: $k_{act}A_T = 0.001\ s^{-1}$; $k_{deact} = 0.1\ s^{-1}$; E = 300; K_D/R_0 = 5; $C_s(t)$ with $k_r = 0.005\ s^{-1}$ and ϵ = 1. Dose magnitudes are λ = 0.1, 0.3, 1, 3, 10, and infinity. Because ϕ is saturable, $\phi_{max} < 1$ for this case.

For signaling through a cytosolic protein as in model 2, we used a sensitivity parameter η to quantify the responsiveness of signal activation to receptor occupancy:

$$\eta = [1 + (E - 1)\phi]; \quad \phi = \frac{S}{K_D + S}. \tag{26}$$

Note that the fractional recruitment ϕ in this model is independent of $C_s(t)$, because we gave S no dependence on receptor occupancy. Two experimentally accessible parameters characterize the responsiveness of signal activation: maximum activation and the peak time.

As stated earlier, the best responsiveness of signaling occurs when $\alpha(t)$ is in pseudoequilibrium with $C_s(t)$. In this optimal scenario, maximum activation $\alpha_{max,\,eq} = k_{act}R_0c_{max}/(k_{act}R_0c_{max} + k_{deact})$, and the signal peak time t_α coincides with t_c, the peak time of receptor occupancy. For various ligand doses, the responsiveness can be assessed through the relative peak activation $\alpha_{max}/\alpha_{max,\,eq}$, and the relative lag time $\Delta\tau_{peak} = (t_\alpha - t_c)/t_c$. Moreover, from Fig. 5 *A* it is apparent that for a given ligand concentration these observables are not independent; as responsiveness decreases, the lag time increases and the peak magnitude decreases.

Because we can now sufficiently characterize the activation profile with two codependent pieces of data, we can now explore the dose-response behavior of model 2 for the kinetic parameters used in Fig. 5 and various values of η. In Fig. 7 *A*, we plot lines of constant λ and η in $\alpha_{max}/\alpha_{max,\,eq}$ versus $\Delta\tau_{peak}$ space, as determined from numerical solutions of Eq. 21. For η = constant, two effects are apparent as we approach saturating ligand concentrations: receptor occupancy peaks increasingly earlier (see Appendix B), making the relative lag time extremely sensitive to the dose, and the relative magnitude of the peak becomes insensitive to dose. Both effects are caused by the fact that ligand association with receptors becomes less of a rate-limiting step as λ is increased.

For a given dose, however, as seen in Fig. 5, both the magnitude and lag time of the signal peak are fairly sensitive to changes in the nature of recruitment, as manifested in the dependence of η on E and ϕ. Fig. 7 *A* effectively defines the requirement for recruitment to achieve certain responsiveness criteria. For example, for a cell responding to growth factor stimulation of λ = 1–10 through model 2, a responsiveness criterion may be $\Delta\tau_{peak} < 1$, in which case η must be >30. Another criterion may be $\alpha_{max}/\alpha_{max,\,eq} > 0.8$, in which case η only need be >10.

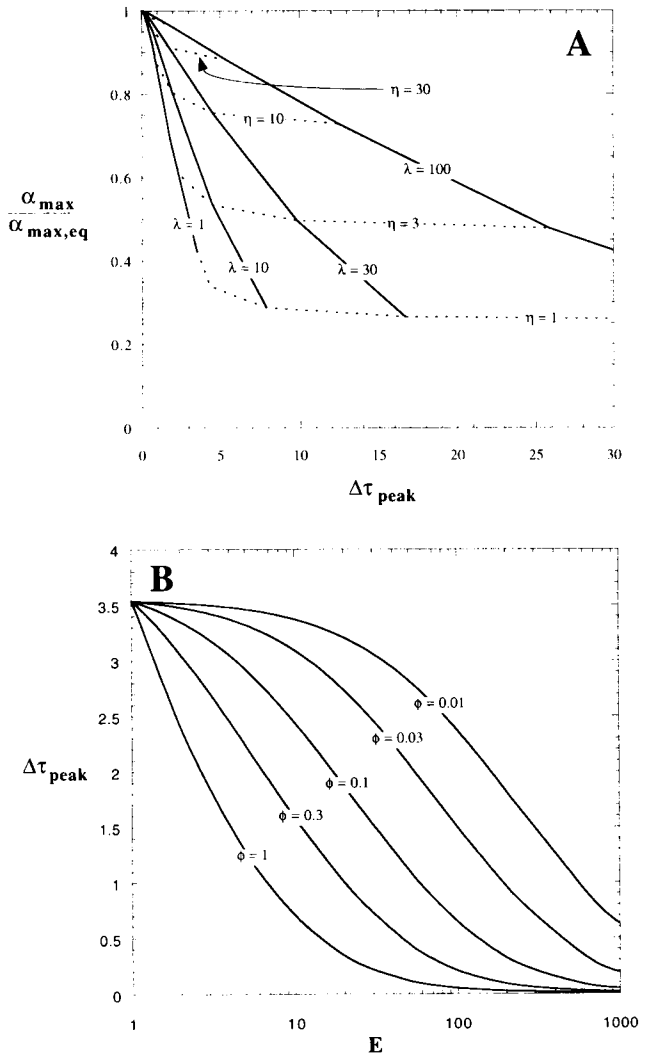

FIGURE 7 Observable sensitivity of Model 2 signal responsiveness to changes in relocation mechanism. The responsiveness of signal transduction in Model 2 to surface receptor stimulation can be characterized by the maximum level of activation α_{max} and the time of the activation peak t_α relative to that of receptor occupancy t_c. In terms of scaled parameters to be used for various ligand doses, we are interested in $\alpha_{max}/\alpha_{max,\,eq}$, where $\alpha_{max,\,eq}$ is the peak activation in the optimal case when α is in equilibrium with $C_s(t)$, and the relative lag time $\Delta\tau_{peak} = (t_\alpha - t_c)/t_c$. (*A*) Dependence of responsiveness criteria on dose and the sensitivity coefficient η. Lines of constant λ and η, are plotted in $\alpha_{max}/\alpha_{max,\,eq}$ versus $\Delta\tau_{peak}$ space for the following parameters as used in Fig. 5: $k_{act}R_0 = 0.001\ s^{-1}$; $k_{deact} = 0.001\ s^{-1}$; $C_s(t)$ with $k_r = 0.005\ s^{-1}$ and $\epsilon = 1$. (*B*) Sensitivity of lag time to changes in relocation mechanism. $\Delta\tau_{peak}$ is plotted versus E for various fractional recruitment values $\phi = S/(K_D + S)$ for the parameters used in *A*, and $\lambda = 1$.

To separate the effects of E and ϕ for model 2 as we did in Fig. 6 for model 1, we plot $\Delta\tau_{peak}$ versus E for $\lambda = 1$, the kinetic parameters used in Fig. 5, and various values of $\phi = S/(K_D + S)$ in Fig. 7 *B*. Again we can see the substantial change in the need for recruitment corresponding to values of E separated by an order of magnitude. For the criterion $\Delta\tau_{peak} < 1$, nearly complete recruitment is required for $E \approx 10$, whereas the requirement for $E \approx 100$ is $\phi \approx 5\%$.

DISCUSSION

A central goal of this paper is to analyze how and why location matters in intracellular signal transduction, using plasma membrane and cytosolic compartments as relevant location categories. We have explored the physical basis for possible enhancements in association rates and equilibrium binding due to relocation of signaling components. By restricting molecules to a thin boundary layer adjacent to a surface, reactants can be greatly concentrated. They may also diffuse more efficiently and over shorter average distances (although less rapidly) in two dimensions to find potential targets. We examined diffusion and reaction mechanisms in the binding of cytosolic and membrane-associated species to a membrane target, and we employed order-of-magnitude reasoning to estimate binding parameters as they might be observed in the cell.

In the diffusion-limited regime, cytosolic proteins likely exhibit an observed forward rate constant of $\sim 10^7\ (Ms)^{-1}$ in associating with a membrane target. As a relevant example, specific recruitment of signaling proteins to phosphotyrosyl motifs of occupied RTKs may reach this limit, because the modular domains responsible for such recruitment events generally exhibit high on and off rates with targets in solution. Most but not all membrane-membrane interactions are expected to be diffusion-limited. Although intuition might suggest that this is due to a reduced molecular mobility in the membrane, a reduction in distance to target and reduction-of-dimensionality often more than compensate for this effect. Rather, the diffusion limitation is caused by a significant reduction in the sampling volume, which increases by 10^2- to 10^3-fold the effective rate constant in the absence of chemical gradients. By comparing the rates of cytosol-membrane and membrane-membrane binding rates, we conclude that relocation from the cytosol to the plasma membrane almost always confers significant enhancement in the protein association rate, by a factor E of ~ 10–1000. The only exception is for diffusion-limited interactions among relatively immobile membrane partners ($D_m/D_c \sim 10^{-3}$), for which E may be as low as ~ 0.1.

More importantly, we also wanted to investigate the potential impact of such enhancements on the dynamics of signal activation. To accomplish this, we considered the enhancement in association rate for a change in location E to be constant, although for membrane relocation E is generally a weak function of target availability. We introduced simple models to illustrate two potential implications of rate enhancement, using the reversible binding of a receptor as the extracellular stimulus.

In model 1, relocation effectively boosts the activation flux of a membrane target molecule, previously at a low steady-state level. Because recruitment is directly tied to receptor occupancy, our signal responds in a dose-dependent manner and is attenuated by receptor down-regulation. This is similar to what is thought to occur in the EGF-mediated activation of Ras (Osterop et al., 1993). Model 1 may also at least qualitatively describe aspects of lipid

second messenger generation through recruitment of cytosolic enzymes such as PI(3)K and phospholipase C-γ (PLC-γ) to occupied RTKs. In the case of PI(3)K, it is likely that both membrane confinement and allosteric changes contribute synergistically to the enhancement of the protein's activity (Klippel et al., 1996); this may be the case for Sos as well (Wang et al., 1995). Using our framework in the estimation of the observed enhancement in association rate E, allosteric changes in binding properties can be incorporated by altering the reaction-limited contribution χ.

In model 2, both fluxes are enhanced by translocation, streamlining the response for maximum efficiency and fidelity with regard to the extracellular input. For high rate enhancements, the signal can constantly adjust to new pseudoequilibria as the level of occupied receptors at the surface rises and falls temporally. For example, the localization of a protein regulated by RTKs and membrane phosphatases (Kulas et al., 1996a,b) may modulate the responsiveness of its signaling profile with time. Although we have examined the modulation of temporal sensitivity in this model, with pseudoequilibrium being the ideal response, still another issue is the sensitivity of the signal output to changes in the input (the balance between membrane-associated activating and deactivating elements). By imposing activation mechanisms that are rapid upon protein association, neglecting possible saturation of the enzymes regulating the signal, the sensitivity of α to C_s at pseudoequilibrium is Michaelian (hyperbolic dependence; Eq. 24). When either or both of the regulatory elements are significantly saturated, a greater sensitivity is achieved where smaller changes in C_s above a threshold level can have a large impact on α (Goldbeter and Koshland, 1981). Because this "zero-order sensitivity" is determined by the substrate concentration relative to the Michaelis constants K_M of the regulatory enzymes, and because substrates can be concentrated by more than an order of magnitude at membrane surfaces, cells may be able to titrate the equilibrium sensitivity of a response by varying membrane recruitment (Appendix D).

Because the way in which a signaling system behaves in response to a stimulus may be crucial to the cell, it must be quantified in such a manner that allows for direct comparisons among different experimental conditions. We have demonstrated that this kind of data can be sensitive to membrane relocation mechanisms for the range of E values typically expected. In particular, for models 1 and 2 there was a distinct shift in the qualitative nature of recruitment required for desirable activation criteria as E moves from $\sim$10 to $>$100.

In model 1, significant recruitment of the cytosolic activating protein is required for severalfold activation of the signal when $E \approx 10$. In contrast, only a small fraction need be relocated for $E \approx 100$ or greater. Relocation in this model is saturable, so the potential for recruitment depends on the dimensionless dissociation constant κ describing the interaction between the cytosolic activator and the specific membrane recruiting element (occupied RTKs in this case). Thus, even at high doses of ligand, only a certain range of fractional recruitment values ϕ may be possible. The actual value of E in a given context thus becomes important in determining signal magnitude. On the other hand, manipulations such as adding lipid modification sequences can yield otherwise unattainable values of ϕ to give responses not seen under normal conditions for a given value of E (e.g., cell transformation).

In model 2, the responsiveness of signal activation to $C_s(t)$ was assessed in terms of the observable magnitude and lag time of the peak activation, and both of these measures were sensitive to aspects of relocation. Of these criteria, a sufficiently small lag time is generally more relevant and was harder to satisfy for a given point in (E, ϕ) space. For the kinetic parameters selected and dimensionless ligand concentration $\lambda = 1$, undesirable responsiveness behavior was seen for $\eta = 1 + (E - 1)\phi < 10$; this result can also be gauged qualitatively from phase information in Fig. 5 *B*. The fractional relocation required to give a certain η is $\phi = (\eta - 1)/(E - 1)$, and so for $E \approx 10$, complete recruitment is required. For $E > 100$, $\phi < 9\%$ for satisfactory behavior.

It is clear from the molecular understanding of signaling that location is important, particularly at the level of membrane interactions. Many key signaling molecules are constitutively targeted to the plasma membrane by posttranslational lipid modifications: the Src tyrosine kinase, heterotrimeric G proteins, and other GTPases such as Ras, Rho, and Rac. Many of these proteins are relatively inactive in solution and cannot function if membrane targeting is prevented. Still others are recruited to the membrane directly or indirectly through interactions between SH2/PTB domains and phosphotyrosine-containing motifs: Sos, phospholipase C-γ (PLC-γ), phosphatidylinositol-3′-kinase (PI(3)K), the Syp tyrosine phosphatase (van der Geer et al., 1994). Interactions with membrane lipids themselves are also important. For example, PLC-γ hydrolyzes phosphatidylinositol-(4′,5′)-diphosphate (PIP_2) to inositol triphosphate and diacylglycerol (DAG). DAG then recruits and activates isoforms of protein kinase C (PKC), a serine-threonine kinase. Other proteins can interact with acidic phospholipids and/or $\beta\gamma$ G-protein subunits, courtesy of pleckstrin homology (PH), or zinc finger protein motifs (Ghosh et al., 1994; Lemmon et al., 1996), which may initiate or stabilize membrane relocation. Further compartmentalization within the plasma membrane has recently been suggested by the selective enrichment of signaling components in membrane pits containing the protein caveolin (Song et al., 1996; Liu et al., 1996; Mineo et al., 1996), which may further concentrate signaling molecules together and/or hinder association with proteins not found in these subdomains.

However, we need not limit our attention to interactions at the plasma membrane or the underlying cytoskeleton. Internalization in endosomes may be effective in concentrating nondissociative ligands and ligand-receptor complexes or sequestering receptors and recruited cytosolic components intracellularly (Baass et al., 1995; see Appen-

dix C). Nuclear translocation is critical for signal transduction at the level of gene regulation; this seems to be important for signaling through MAP kinase, an effector activated by the Ras/Raf pathway (Chen et al., 1992). Two associating proteins can also be anchored to any physical boundary or brought together by some scaffolding mechanism on the molecular level (Faux and Scott, 1996). Indeed, the plasma membrane generally only accounts for a small percentage of the total area associated with cellular membranes and cytoskeletal network surfaces (Gershon et al., 1985; Alberts et al., 1994). As a relevant example, it has been shown recently that MAP kinase associated with microtubules is active (Morishima-Kawashima and Kosik, 1996). For any mechanism, molecular specificity coupled with physical considerations will determine the cellular ramifications of the relocating event. Thus an understanding of the biophysical theory seems appropriate in the interpretation of many experiments in signal transduction.

APPENDIX A: MEAN DIFFUSION TIME WITHIN A BOUNDED CONE TO A SINK AT THE CENTER OF ITS TOP SURFACE

For moderate surface coverages of uniformly distributed, perfectly absorbing sinks on the inside surface of a sphere, the volume afforded each sink can reasonably be defined by a range of angle θ values. For a sink centered on $\theta = 0$, the volume is defined by $|\theta| \le b/a$, where b and a are the half-distance of separation between sink centers and the sphere radius, respectively. Following Eq. 1 for the dimensionless mean time to capture $\tau(r,\theta)$ of randomly distributed molecules contained in the volume,

$$\frac{\partial}{\partial\tilde{r}}\tilde{r}^2\left(\frac{\partial\tau}{\partial\tilde{r}}\right) + \frac{1}{\sin\theta}\frac{\partial}{\partial\theta}\left(\sin\theta\frac{\partial\tau}{\partial\theta}\right) = -\tilde{r}^2$$

$$\left.\frac{\partial\tau}{\partial\theta}\right|_{\theta=0} = \left.\frac{\partial\tau}{\partial\theta}\right|_{\theta=\beta} = 0$$

$$\tau|_{\tilde{r}=0} \text{ finite} \tag{A1}$$

$$\begin{cases}\left.\dfrac{\partial\tau}{\partial\tilde{r}}\right|_{\tilde{r}=1} = 0; & \sigma < \theta < \beta \\ \tau|_{\tilde{r}=1} = 0; & 0 < \theta < \sigma\end{cases}$$

$$\tau \equiv \frac{WD}{a^2}; \quad \tilde{r} \equiv \frac{r}{a}; \quad \beta \equiv \frac{b}{a}; \quad \sigma \equiv \frac{s}{a} \ll 1,$$

where D is the molecular diffusivity of molecules in the volume and s is the sum of the reacting species radii. We can modify the mixed boundary condition at $\tilde{r} = 1$ by assuming an average flux at the sink, its value set to counter the source term (conservation):

$$\left.\frac{\partial\tau}{\partial\tilde{r}}\right|_{\tilde{r}=1} = \begin{cases}0; & \sigma < \theta < \beta \\ -\dfrac{(1-\cos\beta)}{3(1-\cos\sigma)}; & 0 < \theta < \sigma.\end{cases} \tag{A2}$$

We can solve the PDE now to within an additive constant, set by stipulating that the mean capture time averaged over the sink area is zero (Linderman and Lauffenburger, 1986). The resulting mean capture time averaged over space is

$$\bar{\tau} = \frac{1}{15} + \sum_{n=1}^{\infty}\left(\frac{(1-\eta_b)}{3m_n\int_{\eta_b}^{1}P_{m_n}{}^2(\eta)d\eta}\right)\left(\frac{\int_{\eta_s}^{1}P_{m_n}(\eta)d\eta}{(1-\eta_s)}\right)^2$$

$$= \frac{1}{15} + \sum_{n=1}^{\infty}\left[\frac{(2+1/m_n)}{3(1+\eta_b)P_{m_n}(\eta_b)}\left(\left.\frac{d^2P_{m_n}}{d\eta dm_n}\right|_{\eta_b}\right)^{-1}\right]$$

$$\cdot\left[\frac{(1+\eta_s)}{m_n(m_n+1)}\left(\left.\frac{dP_{m_n}}{d\eta}\right|_{\eta_s}\right)\right]^2; \tag{A3}$$

$$\eta = \cos\theta; \quad \eta_b = \cos\beta; \quad \eta_s = \cos\sigma$$

$$\left.\frac{dP_{m_n}}{d\eta}\right|_{\eta_b} = 0,$$

where P_{m_n} are Legendre polynomials and m_n are positive but need not be integral.

Unfortunately, this series does not have desirable convergence properties, and the roots of the transcendental equation become increasingly difficult to determine as we collect terms. A simplifying assumption is to solve A1 with the modification in A2 and $\sin\theta \sim \theta$ ($\beta \sim O(\beta^3)$). The resulting PDE is then scalable ($\tilde{q} \equiv \theta/\alpha$), a major computational advantage:

$$\beta^2\frac{\partial}{\partial\tilde{r}}\tilde{r}^2\left(\frac{\partial\tau}{\partial\tilde{r}}\right) + \frac{1}{\tilde{q}}\frac{\partial}{\partial\tilde{q}}\left(\tilde{q}\frac{\partial\tau}{\partial\tilde{q}}\right) = -\beta^2\tilde{r}^2$$

$$\left.\frac{\partial\tau}{\partial\tilde{q}}\right|_{\tilde{q}=0} = \left.\frac{\partial\tau}{\partial\tilde{q}}\right|_{\tilde{q}=1} = 0$$

$$\left.\frac{\partial\tau}{\partial\tilde{r}}\right|_{\tilde{r}=1} = \begin{cases}0; & \tilde{s} < \tilde{q} < 1 \\ -\dfrac{1}{3\tilde{s}^2}; & 0 < \tilde{q} < \tilde{s}\end{cases} \tag{A4}$$

$$\tilde{s} \equiv \frac{\sigma}{\beta} = \frac{s}{b}.$$

This result is identical to a PDE formulated in conical coordinates, and

$$\bar{\tau} \approx \frac{1}{15} + \sum_{n=1}^{\infty}\frac{4}{3(\lambda_n\tilde{s})^2 f_n(\lambda_n)}\left(\frac{J_1(\lambda_n\tilde{s})}{J_0(\lambda_n)}\right)^2$$

$$J_1(\lambda_n) = 0 \tag{A5}$$

$$f_n(\lambda_n) = \frac{-1+\sqrt{1+4(\lambda_n/\beta)^2}}{2} \cong \frac{\lambda_n}{\beta},$$

where J_n are Bessel functions. If we note that

$$\frac{1}{\sigma N} = \frac{2(1-\cos\beta)}{4\sigma} \approx \frac{\beta^2}{4\sigma} = \frac{\beta}{4\tilde{s}}, \tag{A6}$$

we can construct a mean time that is the sum of a constant and a term inversely proportional to N, as predicted by Eq. 3:

$$\bar{\tau} \approx \frac{1}{15} + \frac{1}{3\sigma N}\sum_{n=1}^{\infty}\frac{16}{\tilde{s}(\lambda_n)^3}\left[\frac{J_1(\lambda_n\tilde{s})}{J_0(\lambda_n)}\right]^2. \tag{A7}$$

This comparison is demonstrated in graphical form as Fig. 8. The apparent advantage of this method is that it allows for interference of the concen-

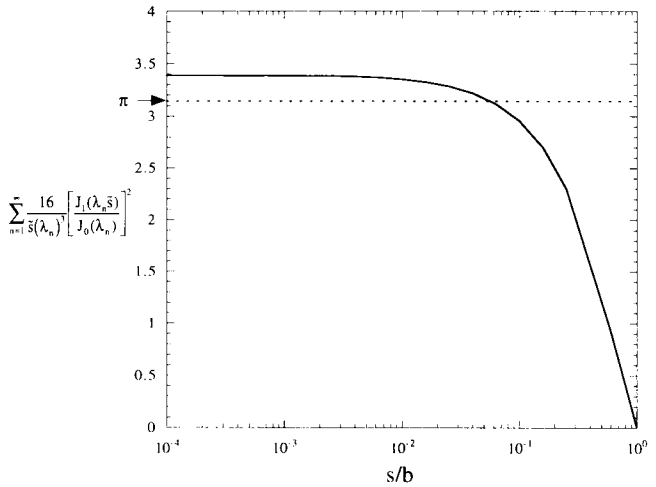

FIGURE 8 Computational analysis of Eq. A7. To determine the approximate mean time to capture of molecules in a conical volume to a sink in the center of the top surface (Eq. A7), the infinite series

$$\sum_{n=1}^{\infty} \frac{16}{\bar{s}(\lambda_n)^3}\left[\frac{J_1(\lambda_n\bar{s})}{J_0(\lambda_n)}\right]^2$$

was estimated, where λ_n are the positive roots of $J_1(\lambda_n) = 0$ and $\bar{s} \equiv s/b$ as defined in the text. Truncation of the series occurred when the magnitude of a term dropped below 10^{-15}. For sparse sinks ($\bar{s} \ll 1$), the concentration gradients around adjacent sinks are independent, and this series converges to a constant. Assuming that the volume is of semiinfinite size yields oblate spheroidal coordinate surfaces and predicts this constant to be π by Eq. 3.

tration profiles by adjacent sinks of finite separation, and thus may be more accurate than Eq. 3 for intermediate sink densities. However, an obvious disadvantage is that Eq. A7 fails to predict exactly the sparse sink limit; because the depletion zone is close to the sink, the approximations made for the concentration profile at the sink introduce noticeable errors. Although the mean capture time averaged over the sink is zero, it is slightly less at $\tilde{q} = 0$ and slightly greater at $\tilde{q} = \bar{s}$. Because capture favors molecules near reflective boundaries, this results in an overestimate (~8%) of $\bar{\tau}(\bar{s} \to 0)$. Using the approximate boundary conditions of Eq. A4, the second term of Eq. A7 in the sparse sink limit approaches $(32/3\pi)/3\sigma N$ (Shoup et al., 1981), rather than $\pi/3\sigma N$, as in Eq. 3.

APPENDIX B: RECEPTOR-LIGAND BINDING AND INTERNALIZATION KINETICS

An extremely simplified model describing the dynamics of surface receptor-ligand complexes C_s and total surface receptors R_T is

$$\begin{aligned} \dot{C}_s &= k_f[L]R_T - (k_f[L] + k_r + k_e)C_s \\ \dot{R}_T &= -k_e C_s \\ C_s(0) &= 0 \\ R_T(0) &= R_0, \end{aligned} \tag{B1}$$

where k_f, k_r, k_e are rate constants describing ligand association, ligand dissociation, and specific complex internalization, respectively, and [L] is the extracellular ligand concentration, assumed to be constant. Such a model neglects de novo receptor synthesis, nonspecific (constitutive) internalization, and intracellular receptor sorting; these are fair simplifications for short periods of stimulation. Also neglected is the saturation of the induced endocytic pathway (Lund et al., 1990). The solution is

$$\begin{aligned} \frac{C_s(t)}{R_0} &= \left(\frac{\lambda}{f_1}\right)\sinh(f_1 k_r t)e^{-f_2 k_r t} \\ \frac{R_T(t)}{R_0} &= \left[\left(\frac{f_2}{f_1}\right)\sinh(f_1 k_r t) + \cosh(f_1 k_r t)\right]e^{-f_2 k_r t} \\ f_1 &= \frac{\sqrt{(1+\lambda+\epsilon)^2 - 4\lambda\epsilon}}{2} \\ f_2 &= \frac{1+\lambda+\epsilon}{2} \\ \lambda &\equiv \frac{k_f[L]}{k_r}; \quad \epsilon \equiv \frac{k_e}{k_r}. \end{aligned} \tag{B2}$$

The activation of the receptor and subsequent auto/transphosphorylation is assumed to be relatively instantaneous upon binding of ligand, and deactivation is considered instantaneous upon ligand dissociation.

The dynamics of $C_s(t)$ follows a biphasic activation profile with time; C_s rises as ligand becomes associated with free receptors, then falls as specific internalization of receptors depletes the total number of surface receptors. The peak value of C_s occurs at a characteristic time t_{peak}:

$$\begin{aligned} C_{s,peak} &= C_s(t_{peak}) \\ t_{peak} &= \frac{\tanh^{-1}(f_1/f_2)}{f_1 k_r}. \end{aligned} \tag{B3}$$

Typical parameters for the well-characterized epidermal growth factor (EGF)/EGF receptor are k_r, $k_e \approx 0.3$ min^{-1} ($\epsilon = 1$) (Lauffenburger and Linderman, 1993). The kinetics of $C_s(t)$ for various values of dimensionless ligand concentration λ are displayed in Fig. 9.

For short time scales ($k_r t$ significantly less than $f_2 - f_1$), note that the level of receptor-ligand complexes can be approximated as a single exponential:

$$\frac{C_s}{R_0} = \left(\frac{\lambda}{2f_1}\right)(1 - e^{-2f_1 k_r t})e^{(f_2 - f_1)k_r t} \approx \left(\frac{\lambda}{2f_1}\right)(1 - e^{-2f_1 k_r t}), \tag{B4}$$

which can simplify the mathematics when the time scale of interest warrants it.

APPENDIX C: SIGNALING THROUGH RECEPTORS IN AN ENDOSOMAL COMPARTMENT

This exercise represents a worst-case scenario for the assumption that signaling through uniformly distributed membrane-associated proteins only occurs at the plasma membrane surface. It is also a strenuous test of whether surface down-regulation can be a primary mechanism for signal attenuation of EGF receptor for relatively short times of stimulation (Osterop et al., 1993).

The total membrane area of sorting endosomes can be conservatively estimated from typical cell dimensions (Lauffenburger and Linderman, 1993) as 1–10% of the plasma membrane area. We can assume that constitutive synthesis, pinocytosis, and recycling have distributed membrane proteins evenly by area for $t < 0$. At $t = 0$, an EGF family ligand is added to the medium, and we are concerned with the activation of receptors and a membrane-associated signaling molecule, both at the surface and in the endosomal compartment, for the first 15 min of stimulation. We consider the kinase domains of internalized receptor/ligand complexes to be unhindered and fully active, and as a worst-case model we neglect

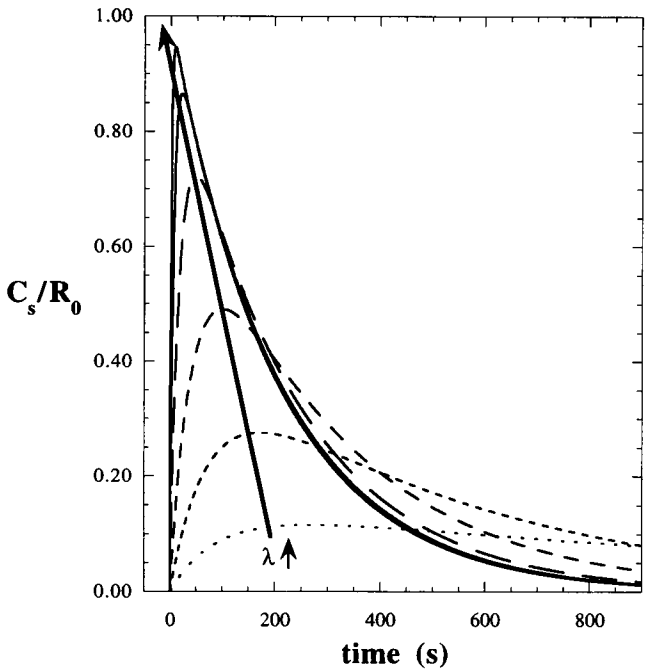

FIGURE 9 Time profiles of C_s, the level of surface receptor-ligand complexes per cell. Equation B2 is plotted for the following parameter values: ligand dissociation rate constant $k_r = 0.005\ s^{-1}$; endocytic rate constant $k_e = 0.005\ s^{-1}$; dimensionless ligand concentrations λ, scaled to the receptor-ligand affinity, of 0.3, 1, 3, 10, 30, and 100. R_0 is the number of free receptors per cell at $t = 0$.

intracellular processing of ligand and receptor. The signaling molecule of interest is regulated by a mechanism as described in Fig. 3 *A*, and the activation rate is enhanced at endosomal surfaces by the same factor E as at the plasma membrane. Employing mass-action kinetics, our transient model is

$$\frac{dC_i}{dt} = k_e C_s - (k_{ri} + k_{fi}[L_i])C_i + k_{fi}[L_i](A_e R_0/A_m - R_T)$$

$$\frac{d[L_i]}{dt} = \frac{1}{N_{Av}V_{end}}[(k_{ri} + k_{fi}[L_i])C_i - k_{fi}[L_i](A_e R_0/A_m - R_T)]$$

$$\frac{d\alpha_s}{dt} = k_{act}A_T\left[1 - \frac{C_i}{K_D + C_i} + (E-1)\frac{C_s}{K_D + C_s}\right] \cdot (1 - \alpha_s) - k_{deact}\alpha_s - k_{er}(\alpha_s - \alpha_i)$$

$$\frac{d\alpha_i}{dt} = k_{act}A_T\left[1 - \frac{C_s}{K_D + C_s} + (E-1)\frac{C_i}{K_D + C_i}\right](1 - \alpha_i) - k_{deact}\alpha_i + k_{er}(\alpha_s - \alpha_i)$$

$$C_i(0) = [L_i](0) = 0; \quad \alpha_s(0) = \alpha_i(0) = \frac{k_{act}A_T}{k_{act}A_T + k_{deact}}, \tag{C1}$$

where $C_s(t)$ and $R_T(t)$ are given in Appendix B, and C_i, $[L_i]$, α_s, and α_i are internalized receptor/ligand complexes, endosomal ligand concentration, percentage activated signal at the surface, and percentage activated signal associated with endosomes, respectively. The rate constants k_e, k_{er}, k_{fi}, and k_{ri} describe induced internalization of surface receptor/ligand complexes, constitutive membrane turnover, receptor-ligand association in endosomes, and receptor/ligand dissociation in endosomes, respectively. A_e/A_m is the ratio of endosomal membrane area (A_e) to plasma membrane area (A_m), taken as 0.1 here to maximize a potential endosomal signaling contribution. N_{Av} is Avogadro's number, and V_{end} is the total volume of endosomes/cell. The parameters E, K_D, k_{act}, A_T, and k_{deact} are as described previously.

The nonlinear ODEs were solved numerically to within 0.001% using the LSODE subroutine on a Sun workstation. Results for typical parameter values and various values of $\lambda = k_f[L]/k_r$ are displayed as Fig. 10; endosomal rate constants k_{fi} and k_{ri} for association/dissociation at pH 6.0 were used to simulate binding of mouse EGF (mEGF) or transforming growth factor-α (TGF-α) (French et al., 1995), and profiles for the less dissociative (mEGF) are displayed in Fig. 10 (there was only slightly less signaling by TGF-α in the model endosomes). Our results suggest that receptor down-regulation of EGF receptor can still be a potent mechanism for the attenuation of signaling at membrane surfaces within the first 10 min of stimulation, whereas endosomes can provide a lower, more sustained level of signaling at later times, as suggested by Baass et al. (1995) (however, effects such as receptor sorting and feedback desensitization of EGF receptor become significant at later times as well). The primary reason for these effects is that the signaling protein of interest is distributed evenly by area in our model through constitutive membrane turnover, with 10% or less present at endosomal surfaces.

However, for cytosolic proteins regulated by the receptor tyrosine kinase (e.g., PLC-γ, PI(3) kinase), this simplistic model would predict a much higher contribution from endosomal versus surface ligand/receptor complexes, and this may offer spatiotemporal specificity for the activation of various signals by the same receptor. Furthermore, membrane proteins

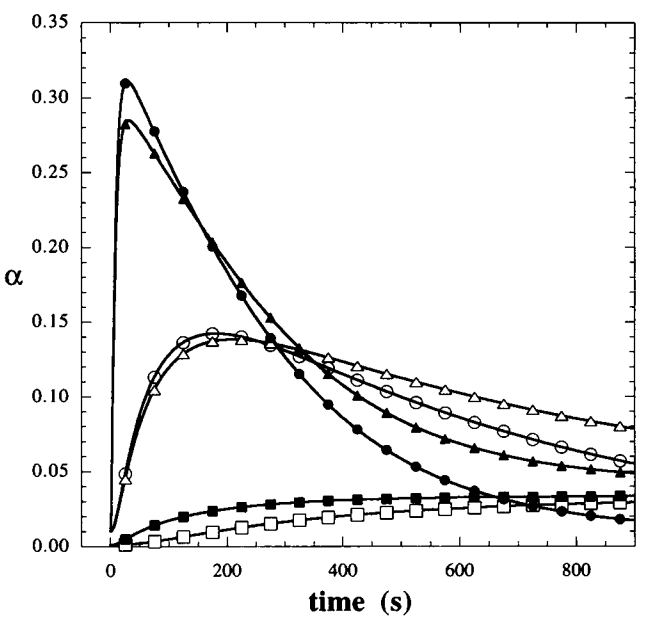

FIGURE 10 Membrane signaling: potential endosomal contribution. The membrane activation model described in Fig. 3 *A* was modified to account for a possible role of internalized EGF/EGF receptor complexes in additional signaling. Our membrane signaling protein of interest is partitioned by area, and the ratio of endosome to surface protein is ~10%. The surface dynamics are described in Appendix B, and the nonlinear ODEs of Eq. C1 were solved numerically for the following parameter values defined in the text: $k_{act}A_T = 0.001\ s^{-1}$; $k_{deact} = 0.1\ s^{-1}$; $K_D/R_0 = 5$; $E = 300$; $k_{fi} = 4.5 \times 10^5\ (Ms)^{-1}$; $k_{ri} = 0.0125\ s^{-1}$; $V_{end} = 10^{-14}$ L; $R_0 = 10^5$/cell; $k_e = 5 \times 10^{-3}\ s^{-1}$; $k_{er} = 5 \times 10^{-4}\ s^{-1}$. ○, □, △, Dimensionless ligand concentration $\lambda = 1$; ●, ■, ▲], $\lambda = 100$. □, ■, $0.1\alpha_i$, endosomal signaling contribution; ▲, △, $0.9\alpha_s + 0.1\alpha_i$, total signal produced; ○, ●, from Fig. 4 *A*, considering plasma membrane dynamics only.

that colocalize with internalizing receptors (e.g., Src) may exhibit an endocytic rate higher than constitutive membrane turnover, leading to enrichment in endosomes alongside the RTK.

In our endocytic compartmentalization model, we assumed that recruitment of activator proteins to membranes via interactions with phosphotyrosine motifs of bound receptors was the same at plasma membrane and endosomal surfaces (as measured by the parameter K_D). This is a function not only of how these proteins recognize such motifs, but also of the phosphotyrosine content at compartmental surfaces as it depends on C_s and C_i. Although this a simplifying assumption, is it valid on experimental and theoretical grounds? There is excellent evidence that this assumption is not exactly accurate.

In one important study (Di Guglielmo et al., 1994), rat livers were bathed in a saturating amount of EGF, and the hepatic plasma membranes and endosomes were fractionated by centrifugation techniques after various times of stimulation. Quantitative biochemical analyses were then performed to ascertain the relative protein amounts and phosphotyrosine content of EGFR and one of its substrates (Shc) associated with the two compartments. After 0.5 min of EGF stimulation, most of the receptors are bound and at the cell surface, whereas at 15 min most of the receptors have down-regulated and are associated with the endosomal fraction. At 0.5 min the specific level of phosphotyrosine (pY/molecule) for Shc is about the same in the two fractions. As the endosomal fraction becomes enriched with receptors, however, the phosphorylation stoichiometry stays about the same at the plasma membrane, but goes up significantly in endosomes. Thus, when almost all receptors are in one fraction or the other, the phosphotyrosine content is different.

Is it possible to explain these observations theoretically? Let us consider pY content to be in rapid equilibrium between RTK and phosphatase activities on the time scale of internalization. For simplicity we will consider the phosphatase activity to operate by a pseudo-first-order mechanism with rate constant k_P, a parameter that does not vary between the two compartments; this would be the case if the phosphatase activity were associated with the cytosol and/or associated with membranes but distributed evenly by constitutive turnover. Next, we will impose saturating conditions under which all receptors inside the cell and at the surface are bound, and allow receptors and receptor substrates to be phosphorylated by both intramolecular (autophosphorylation) and intermolecular (transphosphorylation) events. We can now define P_m and P_e, the specific phosphotyrosine content in the plasma membrane and endosomal compartments, respectively, as a function of the fraction x of receptors that have internalized at any given time. Employing Eq. 10 in the diffusion-limited regime,

$$P_m(x) = \frac{\kappa + \{(2\pi D_m R_0/A_m k_P)(1-x)/\ln[\epsilon_m(1-x)^{-1/2}] - 3/4\}}{1 + \kappa + \{(2\pi D_m R_0/A_m k_P)(1-x)/\ln[\epsilon_m(1-x)^{-1/2}] - 3/4\}}$$

$$P_e(x) = \frac{(\epsilon_e/\epsilon_m)^2\kappa + \{(2\pi D_m R_0/A_m k_P)x/\ln[\epsilon_e x^{-1/2}] - 3/4\}}{(\epsilon_e/\epsilon_m)^2(1+\kappa) + \{(2\pi D_m R_0/A_m k_P)x/\ln[\epsilon_e x^{-1/2}] - 3/4\}},$$

$$\kappa \equiv \frac{k_i}{k_P}; \quad \epsilon_m \equiv \frac{(A_m/\pi R_0)^{1/2}}{s}; \quad \epsilon_e \equiv \frac{(A_e/\pi R_0)^{1/2}}{s} \qquad \text{(C2)}$$

where k_i is the first-order rate constant of the intramolecular kinase mechanism, and A_m, A_e, D_m, R_T, and s are as defined previously. We have assumed that intermolecular transphosphorylation is diffusion-limited because this is what is predicted for most membrane-membrane interactions as described in the text; imposing a second-order reaction-limited rate law does not significantly affect the predicted qualitative behavior. Note that this intermolecular mechanism is conceptually indistinguishable from a dimerization model in which the dimer species has a very short lifetime (Schlessinger, 1979).

In short, this sort of model could explain the results of the fractionation experiment; at relatively sparse receptor densities, such as at the plasma membrane or in endosomes when few of the receptors have internalized, pY stoichiometry can be constant, with intramolecular phosphorylation dominating: $P_m = P_e = \kappa/(1+\kappa)$. At higher receptor densities, such as in the smaller endosomal compartment after significant receptor down-regulation, intermolecular phosphorylation events might become more important, with P_e being a positive function of x. The concentrating effect of the endosome that potentiates this sensitivity is gauged by the ratio of compartment surface areas $(\epsilon_e/\epsilon_m)^2$ (~0.01–0.1 for most cell types). The initial density R_T/A_m is also important in determining whether the cell surface pY stoichiometry is insensitive to down-regulation, and this parameter can vary drastically among different cell/receptor types.

With the distinction between EGFR and EGFR-pY delineated when P_m and P_e are not equivalent, it is more correct to replace C_s and C_i in the model equations governing α_s and α_i (Eq. C1], c and d) with P_mC_s and P_eC_i, respectively, and adjust the common dissociation constant K_D to reflect levels of EGFR-pY. For our simulations, however, this was not incorporated because this model of RTK-phosphatase interplay is highly speculative and would compromise the simplicity of the transient model.

APPENDIX D: MEMBRANE RECRUITMENT AND ZERO-ORDER SENSITIVITY

Our model 2 of membrane signaling involved membrane-associated regulatory elements that activate and deactivate a signaling protein of interest. By imposing a model in which the modification of the protein is concomitant with association of the regulatory elements, the equilibrium response is hyperbolic (Eq. 24). However, in systems in which the signaling protein is covalently modified by positive and negative regulatory enzymes, such as model 2, the state of the signal can achieve a more sensitive, switchlike response to changes in the relative activities of the regulatory elements when either or both enzymes are significantly saturated (Goldbeter and Koshland, 1981). We briefly explore here how membrane recruitment may be able to reversibly modulate a response between hyperbolic and ultrasensitive behaviors.

Consider a signaling protein expressed intracellularly at ~10^4 molecules/cell. At this level, the cytosolic concentration in a typical mammalian cell is ~10 nM. Thus, for significant saturation, one or both of the Michaelis constants K_M must be in the 1 nM range or lower. However, this is hard to achieve for most signaling molecules. If we employ the nomenclature of Goldbeter and Koshland, K_1 and K_2 are the Michaelis constants of the activating and deactivating enzymes, respectively, and ϵ_1 and ϵ_2 are the total enzyme concentrations of the activating and deactivating enzymes, respectively, all scaled to the total substrate concentration W_T. The balance of maximum positive and negative regulatory activities V_1/V_2 is α (not to be confused with the definition of α used in the main text). The mole fraction of unbound, unactivated protein W is then governed by

$$W^3(1-\alpha) + W^2\{K_1 + K_2\alpha + (1-\alpha)[K_1 + \epsilon_1 + \epsilon_2\alpha - 1]\} + K_1W\{(K_1 + \alpha K_2) + (\alpha - 2) + (\epsilon_1 + \epsilon_2\alpha)\} - K_1^2 = 0 \qquad \text{(D1)}$$

with the mole fractions of other species in terms of W; this equation, which accounts for depletion of free substrate due to binding of the enzymes, is taken directly from figure 3 of Goldbeter and Koshland. If we now allow equilibrium partitioning of the substrate between the cytosol and membrane, part of the substrate population will experience a significant reduction in K_1 and K_2 if the regulatory enzymes are both membrane-associated. For example, an observed Michaelis constant (based on whole cell volume) is reduced by the factor E (see main text) when the substrate is modified much more rapidly than it dissociates from the enzyme, whereas it is reduced by the factor χ when the reverse is true. If we assume the former, and that the partition coefficient μ describes the membrane/cytosol ratio of

unbound substrate regardless of activation state, Eq. D1 becomes

$$W_c^3[(1+\mu)(1+\mu E)^2](1-\alpha) + W_c^2\{[(1+\mu)(1+\mu E)] \cdot (K_1 + K_2\alpha) + (1-\alpha)[(1+\mu)(1+\mu E)K_1 + (1+\mu E)^2(\epsilon_1 + \epsilon_2\alpha - 1)]\} + K_1 W_c\{(1+\mu)(K_1 + \alpha K_2) + (1+\mu E)[(\alpha - 2) + (\epsilon_1 + \epsilon_2\alpha)]\} - K_1^2 = 0 \quad \text{(D2)}$$

where W_c is the mole fraction of cytosolic, unbound, unactivated substrate. The fraction of the substrate in the active state is $W_T^* = W_c^* + W_M^* + E_2W_c^* + E_2W_m^*$, the sum of cytosolic and unbound, membrane-associated and unbound, cytosolic and bound, and membrane-associated and bound substrates in the active state. This output of interest can be calculated in terms of W_c:

$$W^*_T = \alpha W_c\left[\frac{K_2(1+\mu)}{K_1 + W_c(1-\alpha)(1+\mu E)} + \frac{\epsilon_2(1+\mu E)}{K_1 + W_c(1+\mu E)}\right]. \quad \text{(D3)}$$

If we consider a case in which $K_1 = K_2 = 3$ (near hyperbolic behavior), and $E = 300$, for example, the cell can achieve observed values of $K_1/E = K_2/E = 0.01$ when all of the substrate is recruited to the membrane ($\mu \gg 1$). If ϵ_1, $\epsilon_2 > 1$, Goldbeter and Koshland showed that an ultrasensitive response is seen under these conditions, as α is modulated from less than to greater than 1. The interesting contribution of membrane recruitment, however, is not simply that zero-order ultrasensitivity can be achieved, but that hyperbolic sensitivity, switchlike sensitivity, and any responses in between can be accessed by modulating the membrane partition coefficient μ.

Financial support from the National Science Foundation Biotechnology Program in the Division of Biological and Environmental Systems to DAL is gratefully acknowledged. JMH was supported by a Graduate Fellowship from the National Science Foundation.

REFERENCES

Adam, G., and M. Delbrück. 1968. Reduction of dimensionality in biological diffusion processes. *In* Structural Chemistry and Molecular Biology. A. Rich and N. Davidson, editors. W. H. Freeman and Co., San Francisco. 198–215.

Alberts, B., D. Bray, J. Lewis, M. Raff, K. Roberts, and J. D. Watson. 1994. Molecular Biology of the Cell, 3rd Ed. Garland Publishing, New York.

Aronheim, A., D. Engelberg, N. Li, N. Al-Alawi, J. Schlessinger, and M. Karin. 1994. Membrane targeting of the nucleotide exchange factor Sos is sufficient for activating the Ras signaling pathway. *Cell.* 78:949–961.

Baass, P. C., G. M. Di Guglielmo, F. Authier, B. I. Posner, and J. J. M. Bergeron. 1995. Compartmentalized signal transduction by receptor tyrosine kinases. *Trends Cell. Biol.* 5:465–470.

Berg, H. C., and E. M. Purcell. 1977. Physics of chemoreception. *Biophys. J.* 20:193–219.

Bos, J. L. 1989. Ras oncogenes in human cancer: a review. *Cancer Res.* 49:4682–4689.

Bourne, H. R., D. A. Sanders, and F. McCormick. 1991. The GTPase superfamily: conserved structure and molecular mechanism. *Nature.* 349:117–127.

Buday, L., and J. Downward. 1993. Epidermal growth factor regulates p21ras through the formation of a complex of receptor, Grb2 adapter protein, and Sos nucleotide exchange factor. *Cell.* 73:611–620.

Carraway, K. L., and C. A. C. Carraway. 1995. Signaling, mitogenesis and the cytoskeleton: where the action is. *BioEssays.* 17:171–175.

Chen, R. H., C. Sarnecki, and J. Blenis. 1992. Nuclear localization and regulation of erk- and rsk-encoded protein kinases. *Mol. Cell. Biol.* 12:915–927.

Cussac, D., M. Frech, and P. Chardin. 1994. Binding of the Grb2 SH2 domain to phosphotyrosine motifs does not change the affinity of its SH3 domains for Sos proline-rich motifs. *EMBO J.* 13:4011–4021.

Di Guglielmo, G. M., P. C. Baass, W. Ou, B. I. Posner, and J. J. M. Bergeron. 1994. Compartmentalization of SHC, GRB2 and mSOS, and hyperphosphorylation of Raf-1 by EGF but not insulin in liver parenchyma. *EMBO J.* 13:4269–4277.

Erickson, J., B. Goldstein, D. Holowka, and B. Baird. 1987. The effect of receptor density on the forward rate constant for binding of ligands to cell surface receptors. *Biophys. J.* 52:657–662.

Faux, M. C., and J. D. Scott. 1996. Molecular glue: kinase anchoring and scaffold proteins. *Cell.* 85:9–12.

Feig, L. A. 1994. Guanine-nucleotide exchange factors: a family of positive regulators of Ras and related GTPases. *Curr. Opin. Cell Biol.* 6:204–211.

Force, T., J. V. Bonventre, G. Heidecker, U. Rapp, J. Avruch, and J. M. Kyriakis. 1994. Enzymatic characteristics of the c-Raf-1 protein kinase. *Proc. Natl. Acad. Sci. USA.* 91:1270–1274.

French, A. R., D. K. Tadaki, S. K. Niyogi, and D. A. Lauffenburger. 1995. Intracellular trafficking of epidermal growth factor family ligands is directly influenced by the pH sensitivity of the receptor/ligand interaction. *J. Biol. Chem.* 270:4334–4340.

Gentry, R., L. Ye, and Y. Nemerson. 1995. Surface-mediated enzymatic reactions: simulations of tissue factor activation of factor X on a lipid surface. *Biophys. J.* 69:362–371.

Gershon, N. D., K. R. Porter, and B. L. Trus. 1985. The cytoplasmic matrix: its volume and surface area and the diffusion of molecules through it. *Proc. Natl. Acad. Sci. USA.* 82:5030–5034.

Ghosh, S., W. Q. Xie, A. F. G. Quest, G. M. Mabrouk, J. C. Strum, and R. M. Bell. 1994. The cysteine-rich region of Raf-1 kinase contains zinc, translocates to liposomes, and is adjacent to a segment that binds GTP-Ras. *J. Biol. Chem.* 269:10000–10007.

Goldbeter, A., and D. E. Koshland, Jr. 1981. An amplified sensitivity arising from covalent modification in biological systems. *Proc. Natl. Acad. Sci. USA.* 78:6840–6844.

Goldstein, B. 1989. Diffusion limited effects of receptor clustering. *Comments Theor. Biol.* 1:109–127.

Hallberg, B., S. I. Rayter, and J. Downward. 1994. Interaction of Ras and Raf in intact mammalian cells upon extracellular stimulation. *J. Biol. Chem.* 269:3913–3916.

Hill, T. L. 1975. Effect of rotation on the diffusion-controlled rate of ligand-protein association. *Proc. Natl. Acad. Sci. USA.* 72:4918–4922.

Hindmarsh, A. C. 1980. LSODE and LSODI, two new initial value ordinary differential equation solvers. *ACM-Signum Newslett.* 15:10–11.

Howe, L. R., S. J. Leevers, N. Gomez, S. Nakielny, P. Cohen, and C. J. Marshall. 1992. Activation of the MAP kinase pathway by the protein kinase raf. *Cell.* 71:335–342.

Jacobson, K., and J. Wojcieszyn. 1984. The translational mobility of substances within the cytoplasmic matrix. *Proc. Natl. Acad. Sci. USA.* 81:6747–6751.

Jelinek, T., P. Dent, T. W. Sturgill, and M. J. Weber. 1996. Ras-induced activation of Raf-1 is dependent on tyrosine phosphorylation. *Mol. Cell. Biol.* 16:1027–1034.

Kikuchi, A., and L. T. Williams. 1994. The post-translational modification of ras p21 is important for Raf-1 activation. *J. Biol. Chem.* 269: 20054–20059.

Klippel, A., C. Reinhard, W. M. Kavanaugh, G. Apell, M. Escobedo, and L. T. Williams. 1996. Membrane localization of phosphatidylinositol 3-kinase is sufficient to activate multiple signal-transducing kinase pathways. *Mol. Cell. Biol.* 16:4117–4127.

Kulas, D. T., G. G. Freund, and R. A. Mooney. 1996a. The transmembrane protein-tyrosine phosphatase CD45 is associated with decreased insulin receptor signaling. *J. Biol. Chem.* 271:755–760.

Kulas, D. T., B. J. Goldstein, and R. A. Mooney. 1996b. The transmembrane protein-tyrosine phosphatase LAR modulates signaling by multiple receptor tyrosine kinases. *J. Biol. Chem.* 271:748–754.

Ladbury, J. E., M. A. Lemmon, M. Zhou, J. Green, M. C. Botfield, and J. Schlessinger. 1995. Measurement of the binding of tyrosyl phosphopeptides to SH2 domains: a reappraisal. *Proc. Natl. Acad. Sci. USA.* 92: 3199–3203.

Lauffenburger, D. A., and J. L. Linderman. 1993. Receptors: Models for Binding, Trafficking, and Signaling. Oxford University Press, New York.

Leevers, S. J., H. F. Paterson, and C. J. Marshall. 1994. Requirement for Ras in Raf activation is overcome by targeting Raf to the plasma membrane. *Nature.* 369:411–414.

Lemmon, M. A., K. M. Ferguson, and J. Schlessinger. 1996. PH domains: diverse sequences with a common fold recruit signaling molecules to the cell surface. *Cell.* 85:621–624.

Linderman, J. J., and D. A. Lauffenburger. 1986. Analysis of intracellular receptor/ligand sorting: calculation of mean surface and bulk diffusion times within a sphere. *Biophys. J.* 50:295–305.

Liu, P., Y. Ying, Y. Ko, and R. G. W. Anderson. 1996. Localization of platelet-derived growth factor-stimulated phosphorylation cascade to caveolae. *J. Biol. Chem.* 271:10299–10303.

Lund, K. A., L. K. Opresko, C. Starbuck, B. J. Walsh, and H. S. Wiley. 1990. Quantitative analysis of the endocytic system involved in hormone-induced receptor internalization. *J. Biol. Chem.* 265: 15713–15723.

Mandiyan, V., R. O'Brien, M. Zhou, B. Margolis, M. A. Lemmon, J. M. Sturtevant, and J. Schlessinger. 1996. Thermodynamic studies of Shc phosphotyrosine interaction domain recognition of the NPXpY motif. *J. Biol. Chem.* 271:4770–4775.

McLaughlin, S., and A. Aderem. 1995. The myristoyl-electrostatic switch: a modulator of reversible protein-membrane interactions. *Trends Biochem. Sci.* 20:272–276.

Mineo, C., G. L. James, E. J. Smart, and R. G. W. Anderson. 1996. Localization of epidermal growth factor-stimulated Ras/Raf-1 interaction to caveolae membrane. *J. Biol. Chem.* 271:11930–11935.

Mochly-Rosen, D. 1995. Localization of protein kinases by anchoring proteins: a theme in signal transduction. *Science.* 268:247–251.

Morishima-Kawashima, M., and K. S. Kosik. 1996. The pool of MAP kinase associated with microtubules is small but constitutively active. *Mol. Biol. Cell.* 7:893–905.

Nesheim, M. E., R. P. Tracy, and K. G. Mann. 1984. "Clotspeed," a mathematical simulation of the functional properties of prothrombinase. *J. Biol. Chem.* 259:1447–1453.

Northrup, S. H., and H. P. Erickson. 1992. Kinetics of protein-protein association explained by Brownian dynamics computer simulation. *Proc. Natl. Acad. Sci. USA.* 89:3338–3342.

Osterop, A. P. R. M., R. H. Medema, G. C. M. van der Zon, J. L. Bos, W. Moller, and J. A. Maassen. 1993. Epidermal growth factor receptors generate Ras-GTP more efficiently than insulin receptors. *Eur. J. Biochem.* 212:477–482.

Pawson, T. 1995. Protein modules and signaling networks. *Nature.* 373: 573–580.

Quilliam, L. A., S. Y. Huff, K. M. Rabun, W. Wei, W. Park, D. Broek, and C. J. Der. 1994. Membrane-targeting potentiates guanine nucleotide exchange factor Cdc25 and Sos1 activation of Ras transforming activity. *Proc. Natl. Acad. Sci. USA.* 91:8512–8516.

Rodriguez-Viciana, P., P. H. Warne, R. Dhand, B. Vanhaesebroeck, I. Gout, M. J. Fry, M. D. Watersfield, and J. Downward. 1994. Phosphatidyl-3-OH kinase as a direct target of Ras. *Nature.* 370:527–532.

Schlessinger, J. 1979. Receptor aggregation as a mechanism for transmembrane signalling: models for hormone action. *In* Physical Chemical Aspects of Cell Surface Events in Cellular Regulation. C. DeLisi and R. Blumenthal, editors. Elsevier North Holland, New York. 89–111.

Shoup, D., G. Lipari, and A. Szabo. 1981. Diffusion-controlled bimolecular reaction rates: the effect of rotational diffusion and orientation constraints. *Biophys. J.* 36:697–714.

Shoup, D., and A. Szabo. 1982. Role of diffusion in ligand binding to macromolecules and cell-bound receptors. *Biophys. J.* 40:33–39.

Song, K. S., S. Li, T. Okamoto, L. A. Quilliam, M. Sargiacomo, and M. P. Lisanti. 1996. Co-purification and direct interaction of Ras with caveolin, an integral membrane protein of caveolae microdomains. *J. Biol. Chem.* 271:9690–9697.

Stokoe, D., S. G. MacDonald, K. Cadwallader, M. Symons, and J. F. Hancock. 1994. Activation of Raf as a result of recruitment to the plasma membrane. *Science.* 264:1463–1467.

Szabo, A., K. Schulten, and Z. Schulten. 1980. First passage time approach to diffusion controlled reactions. *J. Chem. Phys.* 72:4350–4357.

van der Geer, P., T. Hunter, and R. A. Lindberg. 1994. Receptor protein-tyrosine kinases and their signal transduction pathways. *Annu. Rev. Cell Biol.* 10:251–337.

Wang, W., E. M. C. Fisher, Q. Jia, J. M. Dunn, E. Porfiri, J. Downward, and S. E. Egan. 1995. The Grb2 binding domain of mSos1 is not required for downstream signal transduction. *Nature Genet.* 10: 294–300.

Zhou, M. M., J. E. Harlan, W. S. Wade, S. Crosby, K. S. Ravichandran, S. J. Burakoff, and S. W. Fesik. 1995. Binding affinities of tyrosine-phosphorylated peptides to the COOH-terminal SH_2 and NH_2-terminal phosphotyrosine binding domains of Shc. *J. Biol. Chem.* 270: 31119–31123.